



FDTD Schemes for Maxwell's Equations with Embedded Perfect Electric Conductors Based on the Correction Function Method

Yann-Meing Law¹ · Jean-Christophe Nave¹

Received: 6 March 2021 / Revised: 1 July 2021 / Accepted: 12 July 2021 /
Published online: 30 July 2021

© The Author(s), under exclusive licence to Springer Science+Business Media, LLC, part of Springer Nature 2021

Abstract

In this work, we propose staggered FDTD schemes based on the correction function method (CFM) to discretize Maxwell's equations with embedded perfect electric conductor boundary conditions. The CFM uses a minimization procedure to compute a correction to a given FD scheme in the vicinity of the embedded boundary to retain its order. The minimization problem associated with CFM approaches is analyzed in the context of Maxwell's equations with embedded boundaries. In order to obtain a well-posed minimization problem, we propose fictitious interfaces to fulfill the lack of information, namely the surface current and charge density, on the embedded boundary. We introduce CFM-FDTD schemes based on the well-known Yee scheme and a fourth-order staggered FDTD scheme. We investigate the stability of these CFM-FDTD schemes using long time simulations. Convergence studies are performed in 2-D for various geometries of the embedded boundary. CFM-FDTD schemes have shown high-order convergence.

Keywords Embedded perfect electric conductor · Maxwell's equations · Correction function method · Finite-difference time-domain · High order

Mathematics Subject Classification 35Q61 · 65M06 · 78M20

1 Introduction

In electromagnetic dynamics, the perfect electric conductor is an important idealized material that allows surface charges and currents. Since the surface charge and current density are often unknown, PEC walls are modeled through the imposition of boundary conditions that

✉ Yann-Meing Law
yann-meing.law-kamcio@mail.mcgill.ca

Jean-Christophe Nave
jean-christophe.nave@mcgill.ca

¹ Department of Mathematics and Statistics, McGill University, Montréal, QC H3A 0B9, Canada

require the continuity of the normal component of the magnetic field and the tangential component of the electric field on the boundary of a domain [3,13].

In free-space simulations involving PECs, the interface between a PEC and its surrounding medium is treated as an embedded boundary. Embedded boundary conditions can be difficult to treat, particularly in a finite-difference context. Indeed, challenges include the development of numerical methods that can handle various complex geometries of the PEC without increasing the complexity of a numerical method while retaining high-order accuracy. It is also worth mentioning that high-order schemes are important to diminish the phase error for long time simulations [13].

Many numerical strategies are proposed to achieve high-order accuracy for problems involving embedded PEC walls, such as discontinuous Galerkin (DG) approaches [14], pseudospectral time-domain methods (PSTD) [9,10,26] or finite-difference time-domain (FDTD) schemes [8,17,24,28,31]. A discontinuous Galerkin approach can treat complex geometries of embedded PEC walls by an appropriate mesh. However, a large number of unknowns for high-order accuracy is needed for these approaches. This is due to the use of piecewise polynomial spaces that do not require continuity between two elements of a mesh. Various strategies have been proposed to reduce the computational cost of DG based methods, such as parallel computing strategies or particular choices of basis functions [6,7]. It is also worth mentioning that finite-element approaches with non-body-fitted grids have been developed for electromagnetic problems, but low-order basis functions have been used [4,5,25]. On the other hand, finite-difference time-domain approaches use a simple Cartesian grid and have low computational costs. However, the imposition of embedded boundary conditions is far from trivial. A naive approach is to use the Yee scheme [27] with a staircased approximation of the embedded boundary. Unfortunately, this approach leads to a first-order scheme at best and sometimes to non-convergent approximations [8]. To overcome this issue, many FDTD approaches have been proposed, such as overlapping grids [28], contour path methods [17,24] and locally modifications of FD schemes [8,31]. A staircase-free FDTD scheme has been proposed in [8] to recover a second-order scheme without significantly compromising the simplicity of the used FD scheme. They explicitly impose PEC boundary conditions by locally modifying a finite-difference scheme in the vicinity of the boundary. Following the same idea, a fourth-order finite-difference scheme based on the Matched Interface and Boundary (MIB) method [32] has been proposed to handle embedded PEC walls using the vector Helmholtz equation [31]. This FD scheme is obtained by deriving and explicitly imposing jump conditions for PEC walls on the embedded boundary. However, the complexity of a MIB based scheme increases with its order or the complexity of the geometry of the embedded boundary because of the imposition of high-order jump conditions [29,30]. Finally, pseudospectral methods have the advantage to require less grid points per wavelength than FDTD approaches. The Fourier and Chebyshev collocation methods with a multidomain strategy have been used to achieve high-order accuracy [9,26]. These approaches need a multidomain decomposition with an appropriate mesh grid for embedded boundary conditions, and therefore an additional treatment of interfaces between subdomains is needed. An alternative approach is to use a Fourier penalty method [10]. Although this approach does not need a multidomain strategy, there are some stability issues that limit the order of the method in two and three dimensions.

Another avenue to handle embedded boundary conditions is FD schemes based on the Correction Function Method (CFM). The CFM, which was inspired by the Ghost Fluid Method (GFM), has been originally developed to treat Poisson's equations with interface jump conditions with arbitrarily complex interfaces. FD schemes based on the CFM achieve high-order by means of a minimization problem. This numerical strategy has been successfully applied to Poisson problems with constant and piecewise constant coefficients, and interface jumps

[20,21]. It is also worth mentioning that a CFM based strategy has also been used to treat 3-D Poisson equation with interface jump conditions [22]. Afterward, extensions of this method have been used to handle the wave equation and Maxwell's equations with constant coefficients and interface jump conditions [2,19]. Briefly, the underline assumption of the CFM is that jumps on the interface can be smoothly extended in the vicinity of the interface. Therefore, a system of partial differential equations (PDEs) coming from the original system of PDEs is derived to model jumps around the interface. The solution of this system of PDEs is called the correction function. A square measure of the error associated with the correction function's system of PDEs is then minimized to compute approximations of the correction function. Afterward, these approximations are used to correct a given FD scheme that involves nodes in different subdomains. It is worth mentioning that the additional computational cost associated with minimization problems of the CFM is not negligible. Hence, this makes the use of parallel computing strategies unavoidable [1].

As mentioned before, a FDTD strategy based on the CFM has been developed to handle Maxwell's equations with constant coefficients and interface jump conditions [19]. Even though this numerical scheme could also be used to enforce embedded boundary conditions, one needs to impose all information on the boundary, that is both normal and tangential components of each electromagnetic field. This is a major drawback when embedded PEC wall boundary conditions are considered. As shown in this work, a direct application of the numerical scheme proposed in [19] for PEC wall boundary conditions leads to an ill-posed minimization problem because of the lack of information on the embedded boundary. Hence, the main goal of this work is to overcome this issue and proposes high-order FDTD schemes based on the CFM, which are referred as CFM-FDTD schemes, to handle embedded PEC wall boundary conditions. The algorithm presented in this paper also provides an important stepping stone towards a CFM-FDTD approach to handle Maxwell's interface problems.

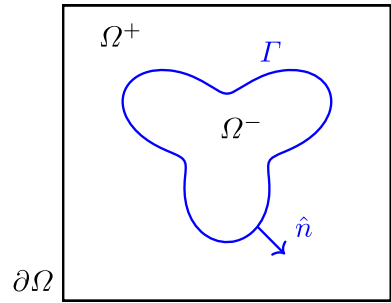
We first extend CFM-FDTD schemes for PEC problems for which the surface current and charge density are unknown. Afterward, we describe a construction of appropriate local patches that are needed for minimization problems. This construction reduces the computation cost of the CFM while guaranteeing the uniqueness of the correction function for a given node to be corrected. We then introduce CFM-FDTD schemes based on the well-known Yee scheme and a fourth-order staggered FDTD scheme. Finally, numerical examples based on the transverse magnetic (TM_z) and electric (TE_z) modes are performed to verify the proposed CFM-FDTD schemes.

The paper is organized as follows. In Sect. 2, we introduce Maxwell's equations with embedded PEC wall conditions. The CFM applied to Maxwell's equations is presented in Sect. 3. In this section, we propose an extension of the CFM for problems involving a PEC for which the surface current and charge density are unknown. The minimization problems coming from the CFM are analyzed. The impact of the CFM on a FDTD scheme is also investigated and the construction of local patches is described. We then introduce CFM-FDTD schemes based on the Yee scheme in Sect. 4 and on a fourth-order staggered FDTD scheme in Sect. 5. Finally, we perform numerical examples to verify the proposed CFM-FDTD schemes in both Sects. 6 and 7.

2 Definition of the Problem

Assume a domain Ω subdivided into two subdomains Ω^+ and Ω^- . The interface Γ between subdomains is independent of time and allows solutions, that is the magnetic field \mathbf{H} and

Fig. 1 Geometry of a domain Ω with an interface Γ



the electric field \mathbf{E} in this work, to be discontinuous along it. We define \mathbf{H}^+ and \mathbf{E}^+ as the solutions in Ω^+ , and \mathbf{H}^- and \mathbf{E}^- as the solutions in Ω^- . The jumps are denoted as

$$\begin{aligned} \llbracket \mathbf{H} \rrbracket &= \mathbf{H}^+ - \mathbf{H}^-, \\ \llbracket \mathbf{E} \rrbracket &= \mathbf{E}^+ - \mathbf{E}^-. \end{aligned}$$

We consider the boundary $\partial\Omega$ of Ω and a given time interval $I = [0, T]$. Assuming linear media and a periodic domain, Maxwell’s equations with interface conditions are given by

$$\partial_t(\mu \mathbf{H}) + \nabla \times \mathbf{E} = 0 \quad \text{in } \Omega \times I, \tag{1a}$$

$$\partial_t(\epsilon \mathbf{E}) - \nabla \times \mathbf{H} = 0 \quad \text{in } \Omega \times I, \tag{1b}$$

$$\nabla \cdot (\epsilon \mathbf{E}) = \rho \quad \text{in } \Omega \times I, \tag{1c}$$

$$\nabla \cdot (\mu \mathbf{H}) = 0 \quad \text{in } \Omega \times I, \tag{1d}$$

$$\hat{\mathbf{n}} \times \llbracket \mathbf{E} \rrbracket = 0 \quad \text{on } \Gamma \times I, \tag{1e}$$

$$\hat{\mathbf{n}} \times \llbracket \mathbf{H} \rrbracket = \mathbf{J}_s(\mathbf{x}, t) \quad \text{on } \Gamma \times I, \tag{1f}$$

$$\hat{\mathbf{n}} \cdot \llbracket \epsilon \mathbf{E} \rrbracket = \rho_s(\mathbf{x}, t) \quad \text{on } \Gamma \times I, \tag{1g}$$

$$\hat{\mathbf{n}} \cdot \llbracket \mu \mathbf{H} \rrbracket = 0 \quad \text{on } \Gamma \times I, \tag{1h}$$

$$\mathbf{H}(\mathbf{x}, 0) = \mathbf{H}_0(\mathbf{x}) \quad \text{in } \Omega, \tag{1i}$$

$$\mathbf{E}(\mathbf{x}, 0) = \mathbf{E}_0(\mathbf{x}) \quad \text{in } \Omega, \tag{1j}$$

where μ is the magnetic permeability, ϵ is the electric permittivity, ρ is the electric charge density, \mathbf{J}_s is the surface current density, ρ_s is the surface charge density and $\hat{\mathbf{n}}$ is the unit normal to the interface Γ pointing toward Ω^+ . Figure 1 illustrates a typical geometry of a domain Ω . Without loss of generality, we assume constant coefficients that are such that $\epsilon, \mu > 0$ and $\rho = 0$.

For problems involving a PEC, we often do not know the surface current density \mathbf{J}_s and the surface charge density ρ_s . Interface conditions (1e)–(1h) are then reduced to

$$\hat{\mathbf{n}} \times \llbracket \mathbf{E} \rrbracket = 0 \quad \text{on } \Gamma \times I,$$

$$\hat{\mathbf{n}} \cdot \llbracket \mu \mathbf{H} \rrbracket = 0 \quad \text{on } \Gamma \times I.$$

Let us assume that subdomain Ω^- is a PEC, we then have $\mathbf{E}^-(\mathbf{x}, t) = 0, \forall(\mathbf{x}, t) \in \Omega^- \times I$. Considering that the initial condition of the magnetic field is given by $\mathbf{H}^-(\mathbf{x}, 0) = 0$ [3,16], we also have $\mathbf{H}^-(\mathbf{x}, t) = 0, \forall(\mathbf{x}, t) \in \Omega^- \times I$. Thus, interface conditions on Γ can be considered as embedded boundary conditions, given by

$$\begin{aligned} \hat{\mathbf{n}} \times \mathbf{E}^+ &= 0 \quad \text{on } \Gamma \times I, \\ \hat{\mathbf{n}} \cdot (\mu \mathbf{H}^+) &= 0 \quad \text{on } \Gamma \times I, \end{aligned} \tag{2}$$

for Ω^+ . In this work, we focus on problems involving PECs and therefore assume Γ to be an embedded boundary of Ω^+ . For further discussions on Maxwell’s equations with PEC boundary conditions (2) and results on its well-posedness, we refer the interested reader to [3].

3 Correction Function Method

The smoothness of solutions is important when one wants to use FD schemes. Realizing that problem (1) can have discontinuous solutions, standard FD schemes cannot a priori be used around the embedded boundary Γ . The Correction Function Method allows one to circumvent this issue. The purpose of the CFM is to find a correction for a finite difference approximation that involves nodes that belong to different subdomains. To find such a correction, the CFM assumes that solutions in $\Omega^+ \times I$ and $\Omega^- \times I$ can be smoothly extended in a small region $\Omega_\Gamma \times I$, where $\Omega_\Gamma \subset \Omega$ encloses the embedded boundary Γ , in such a way that the original PDE is still satisfied. A functional that is a square measure of the error of a PDE that describes the behaviour of jumps or correction functions in the vicinity of the embedded boundary is derived. This functional is then minimized in a discrete functional space to obtain approximations of the correction function in $\Omega_\Gamma \times I$. In practice, we define a local patch $\Omega_\Gamma^h \subset \Omega_\Gamma$ for which the correction function needs to be computed at a node $\mathbf{x}_c \in \Omega_\Gamma^h$ and a time interval $I_\Gamma^h = [t_n - \Delta t_\Gamma, t_n]$. The additional computational cost associated with the CFM is not negligible when compared with the original FDTD scheme. In fact, the CFM consumes most of the computational time. However, a parallel implementation of the computation of correction functions can be performed since minimization problems associated with local patches are independent. We refer to [1] for more details about the benefits of a parallel implementation of the CFM.

In the following, we summarize the procedure for the CFM applied on Maxwell’s equations when electromagnetic fields are known on the embedded boundary [19]. Afterward, we present an analysis of the minimization problem that is needed for the CFM. The functional to be minimized is then modified and analyzed for embedded PEC walls for which the surface current and charge density are unknown. We also investigate the impact of such a modification on a FDTD scheme. We then describe a construction of local patches that reduces the computation cost of the CFM and ensures an appropriate representation of the embedded boundary within the local patch.

Let us first introduce some notations. The inner product in $L^2(\Omega_\Gamma^h \times I_\Gamma^h)$ is defined by

$$\langle \mathbf{v}, \mathbf{w} \rangle = \int_{I_\Gamma^h} \int_{\Omega_\Gamma^h} \mathbf{v} \cdot \mathbf{w} \, dV \, dt$$

and we also use the notation

$$\langle \mathbf{v}, \mathbf{w} \rangle_\Gamma = \int_{I_\Gamma^h} \int_{\Omega_\Gamma^h \cap \Gamma} \mathbf{v} \cdot \mathbf{w} \, dS \, dt$$

for legibility. The correction functions are defined as

$$\begin{aligned} \mathbf{D}_H &= \mathbf{H}^+ - \mathbf{H}^-, \\ \mathbf{D}_E &= \mathbf{E}^+ - \mathbf{E}^-. \end{aligned}$$

Let us first assume that the surface current density and charge density are known. Following the same procedure as in [19], one can obtain the following quadratic functional to minimize

$$\begin{aligned}
 J(\mathbf{D}_H, \mathbf{D}_E) &= \frac{\ell_h}{2} \langle \mu \partial_t \mathbf{D}_H + \nabla \times \mathbf{D}_E, \mu \partial_t \mathbf{D}_H + \nabla \times \mathbf{D}_E \rangle \\
 &+ \frac{\ell_h}{2} \langle \epsilon \partial_t \mathbf{D}_E - \nabla \times \mathbf{D}_H, \epsilon \partial_t \mathbf{D}_E - \nabla \times \mathbf{D}_H \rangle \\
 &+ \frac{c_p}{2} \langle \hat{\mathbf{n}} \times \mathbf{D}_H - \mathbf{J}_s, \hat{\mathbf{n}} \times \mathbf{D}_H - \mathbf{J}_s \rangle_\Gamma + \frac{c_p}{2} \langle \hat{\mathbf{n}} \cdot \mathbf{D}_H, \hat{\mathbf{n}} \cdot \mathbf{D}_H \rangle_\Gamma \\
 &+ \frac{c_p}{2} \langle \hat{\mathbf{n}} \times \mathbf{D}_E, \hat{\mathbf{n}} \times \mathbf{D}_E \rangle_\Gamma + \frac{c_p}{2} \langle \hat{\mathbf{n}} \cdot \mathbf{D}_E - \frac{\rho_s}{\epsilon}, \hat{\mathbf{n}} \cdot \mathbf{D}_E - \frac{\rho_s}{\epsilon} \rangle_\Gamma,
 \end{aligned}$$

where $c_p > 0$ is a penalization coefficient and ℓ_h is the length in space of the patch. We scale the integral over the domain by ℓ_h to ensure that all terms in the functional J behave in a similar way when the computational grid is refined [19]. To guarantee the divergence-free constraint (1c) and (1d), we minimize the functional J in a divergence-free space-time polynomial space, namely

$$V = \{ \mathbf{v} \in [P^k(\Omega_T^h \times I_T^h)]^3 : \nabla \cdot \mathbf{v} = 0 \},$$

where P^k denotes the space of polynomials of degree k . It is worth mentioning that basis functions of V are based on high-degree divergence-free basis functions proposed in [6] for discontinuous Galerkin approaches. The problem statement is then

$$\text{Find } (\mathbf{D}_H, \mathbf{D}_E) \in V \times W \text{ such that } (\mathbf{D}_H, \mathbf{D}_E) \in \underset{\mathbf{v} \in V, \mathbf{w} \in W}{\arg \min} J(\mathbf{v}, \mathbf{w}), \tag{3}$$

where $W = V$. The following proposition shows that the quadratic functional J has a global minimizer when finite-dimensional functional spaces are used and for an appropriate choice of the penalization coefficient c_p .

Proposition 1 *Let us consider problem (3), and assume \mathbf{v} and \mathbf{w} to be basis functions of V and W . There exists a positive constant $\tilde{c} = \frac{c_p}{\ell_h}$ for which the functional J has a unique global minimizer.*

Proof Let us first notice that problem (3) is an unconstrained minimization problem. In this case, if the Hessian matrix coming from a quadratic functional is positive definite, then the critical point is a global minimum. Let us consider \mathbf{v} and \mathbf{w} to be basis functions of V and W . The Hessian matrix coming from problem (3) is given by

$$\begin{bmatrix} \ell_h a + c_p b & \ell_h e \\ \ell_h e & \ell_h c + c_p d \end{bmatrix},$$

where

$$\begin{aligned}
 a &= \langle \mu \partial_t \mathbf{v}, \mu \partial_t \mathbf{v} \rangle + \langle \nabla \times \mathbf{v}, \nabla \times \mathbf{v} \rangle, \\
 b &= \langle \hat{\mathbf{n}} \times \mathbf{v}, \hat{\mathbf{n}} \times \mathbf{v} \rangle_\Gamma + \langle \hat{\mathbf{n}} \cdot \mathbf{v}, \hat{\mathbf{n}} \cdot \mathbf{v} \rangle_\Gamma, \\
 c &= \langle \nabla \times \mathbf{w}, \nabla \times \mathbf{w} \rangle + \langle \epsilon \partial_t \mathbf{w}, \epsilon \partial_t \mathbf{w} \rangle, \\
 d &= \langle \hat{\mathbf{n}} \times \mathbf{w}, \hat{\mathbf{n}} \times \mathbf{w} \rangle_\Gamma + \langle \hat{\mathbf{n}} \cdot \mathbf{w}, \hat{\mathbf{n}} \cdot \mathbf{w} \rangle_\Gamma, \\
 e &= \langle \mu \partial_t \mathbf{v}, \nabla \times \mathbf{w} \rangle - \langle \epsilon \partial_t \mathbf{w}, \nabla \times \mathbf{v} \rangle.
 \end{aligned}$$

Requiring the Hessian matrix to be positive definite, one finds the following conditions:

$$\ell_h a + c_p b > 0, \tag{4}$$

$$(\ell_h a + c_p b) (\ell_h c + c_p d) - (\ell_h e)^2 > 0. \tag{5}$$

Since \mathbf{v} and \mathbf{w} are basis functions of V and W , we have $\mathbf{v} \neq 0$ and $\mathbf{w} \neq 0$. Noticing that \mathbf{v} and \mathbf{w} cannot be both orthogonal and collinear to $\hat{\mathbf{n}}$ except for the zero element, we also have $b \neq 0$ and $d \neq 0$. Hence, condition (4) is always satisfied. However, condition (5) leads to the following criterion

$$\tilde{c} > \frac{e^2 - ac}{\tilde{c}bd} - \frac{ad + bc}{bd}, \tag{6}$$

where $\tilde{c} = \frac{c_p}{\ell_h}$. For a sufficiently large \tilde{c} , criterion (6) is satisfied. □

Let us now investigate the impact of the CFM based on minimization problem (3) on a given FD scheme. Assume a spatial finite difference operator noted L , such that

$$\partial_t \mathbf{U}(t) + L \mathbf{U}(t) = 0, \tag{7}$$

where \mathbf{U} is a vector containing m unknowns that estimate electromagnetic fields on the grid points in space. We consider that a correction is needed at r nodes in the vicinity of the embedded boundary, system (7) then becomes

$$\partial_t \mathbf{U}(t) + L \mathbf{U}(t) + L A \mathbf{D}(t) = 0, \tag{8}$$

where \mathbf{D} is a vector containing r values of the correction function coming from problem (3) and A is a rectangular matrix of dimension $m \times r$ with either 0 or ± 1 as components depending on where the correction is needed. Hence, the correction function can therefore be considered as a time-dependent force term. From Proposition 1, we have the existence and unicity of the coefficients of polynomial approximations of the correction function for an appropriate c_p . Since $\mathbf{D}_H(\mathbf{x}, t)$ and $\mathbf{D}_E(\mathbf{x}, t)$ are polynomial functions, and $\Omega_\Gamma^h \times I_\Gamma^h$ is a compact domain, these approximations and their derivatives are bounded in the infinity norm. It is therefore sufficient to investigate the stability of the original FDTD scheme (7) to identify any time-step criteria of the corresponding CFM-FDTD scheme (see Theorem 5.1.1 in [12]). As for the consistency, it can be shown that the order in space of a CFM-FDTD scheme is $\min\{k, n\}$, where k is the degree of polynomial approximations of the correction function and n is the order of the FD scheme in space (see Proposition 3).

3.1 PEC Wall Boundary Conditions

Let us now focus on PEC wall boundary conditions. By Proposition 1, one cannot just neglect interface conditions (1f) and (1g) for PEC problems for which \mathbf{J}_s and ρ_s are unknown because this leads to an ill-posed minimization problem. To circumvent this issue, we propose to use fictitious interfaces on which we enforce these conditions

$$\begin{aligned} \hat{\mathbf{n}}_{1,i} \times (\mathbf{E}^+ - \mathbf{E}^*) &= 0 \quad \text{on } \Gamma_{1,i} \times I \quad \text{for } i = 1, \dots, N_1, \\ \hat{\mathbf{n}}_{2,i} \times (\mathbf{H}^+ - \mathbf{H}^*) &= 0 \quad \text{on } \Gamma_{2,i} \times I \quad \text{for } i = 1, \dots, N_2, \\ \hat{\mathbf{n}}_{3,i} \cdot (\mathbf{E}^+ - \mathbf{E}^*) &= 0 \quad \text{on } \Gamma_{3,i} \times I \quad \text{for } i = 1, \dots, N_3, \\ \hat{\mathbf{n}}_{4,i} \cdot (\mathbf{H}^+ - \mathbf{H}^*) &= 0 \quad \text{on } \Gamma_{4,i} \times I \quad \text{for } i = 1, \dots, N_4, \end{aligned} \tag{9}$$

where N_k is the number of fictitious interfaces $\Gamma_{k,i} \subset \Omega^+ \cap \Omega_\Gamma^h$ for $k = 1, \dots, 4$, $\hat{\mathbf{n}}_{k,i}$ is the unit normal associated with fictitious interface $\Gamma_{k,i}$, and \mathbf{H}^* and \mathbf{E}^* are respectively finite difference approximations of \mathbf{H}^+ and \mathbf{E}^+ in Ω^+ . In Sect. 3.2, we provide more details

on the implementation of these fictitious interface conditions. The functional to minimize is then given by

$$\begin{aligned}
 \tilde{J}(\mathbf{D}_H, \mathbf{D}_E) &= \frac{\ell_h}{2} \langle \mu \partial_t \mathbf{D}_H + \nabla \times \mathbf{D}_E, \mu \partial_t \mathbf{D}_H + \nabla \times \mathbf{D}_E \rangle \\
 &+ \frac{\ell_h}{2} \langle \epsilon \partial_t \mathbf{D}_E - \nabla \times \mathbf{D}_H, \epsilon \partial_t \mathbf{D}_E - \nabla \times \mathbf{D}_H \rangle \\
 &+ \frac{c_p}{2} \langle \hat{\mathbf{n}} \times \mathbf{D}_E, \hat{\mathbf{n}} \times \mathbf{D}_E \rangle_\Gamma + \frac{c_p}{2} \langle \hat{\mathbf{n}} \cdot \mathbf{D}_H, \hat{\mathbf{n}} \cdot \mathbf{D}_H \rangle_\Gamma \\
 &+ \frac{c_f}{2N_E} \sum_{i=1}^{N_1} \langle \hat{\mathbf{n}}_{1,i} \times (\mathbf{D}_E - \mathbf{E}^*), \hat{\mathbf{n}}_{1,i} \times (\mathbf{D}_E - \mathbf{E}^*) \rangle_{\Gamma_{1,i}} \\
 &+ \frac{c_f}{2N_H} \sum_{i=1}^{N_2} \langle \hat{\mathbf{n}}_{2,i} \times (\mathbf{D}_H - \mathbf{H}^*), \hat{\mathbf{n}}_{2,i} \times (\mathbf{D}_H - \mathbf{H}^*) \rangle_{\Gamma_{2,i}} \\
 &+ \frac{c_f}{2N_E} \sum_{i=1}^{N_3} \langle \hat{\mathbf{n}}_{3,i} \cdot (\mathbf{D}_E - \mathbf{E}^*), \hat{\mathbf{n}}_{3,i} \cdot (\mathbf{D}_E - \mathbf{E}^*) \rangle_{\Gamma_{3,i}} \\
 &+ \frac{c_f}{2N_H} \sum_{i=1}^{N_4} \langle \hat{\mathbf{n}}_{4,i} \cdot (\mathbf{D}_H - \mathbf{H}^*), \hat{\mathbf{n}}_{4,i} \cdot (\mathbf{D}_H - \mathbf{H}^*) \rangle_{\Gamma_{4,i}},
 \end{aligned} \tag{10}$$

where $c_f > 0$ and $c_p > 0$ are penalization coefficients, and $N_H = N_2 + N_4$ and $N_E = N_1 + N_3$ are the total numbers of fictitious interfaces for each electromagnetic field. The use of fictitious interface conditions (9) with Maxwell’s equations in functional (10) implicitly estimates \mathbf{J}_s and ρ_s on the embedded boundary. From this perspective, these conditions fulfill the lack of information on the embedded boundary. The problem statement is then

$$\text{Find } (\mathbf{D}_H, \mathbf{D}_E) \in V \times W \text{ such that } (\mathbf{D}_H, \mathbf{D}_E) \in \underset{\mathbf{v} \in V, \mathbf{w} \in W}{\arg \min} \tilde{J}(\mathbf{v}, \mathbf{w}), \tag{11}$$

where $W = V$. The following proposition guarantees that there is a global minimizer for an appropriate choice of the penalization coefficient c_f and fictitious interfaces.

Proposition 2 *Let us consider problem (11), and assume \mathbf{v} and \mathbf{w} to be basis functions of V and W . Moreover, assume that there are collinear and orthogonal fictitious interfaces to each plane defined by the axis of the Cartesian coordinate system and for each type of fictitious interface conditions (9). There exists a positive constant $\tilde{c} = \frac{c_f}{\ell_h}$ for which the functional \tilde{J} has a unique global minimizer.*

Proof The demonstration is similar to the proof presented in Proposition 1. The Hessian matrix coming from problem (11) is given by

$$\begin{bmatrix} \ell_h a + c_p b + c_f \tilde{b} & \ell_h e \\ \ell_h e & \ell_h c + c_p d + c_f \tilde{d} \end{bmatrix},$$

where a , c and e are the same as in Proposition 1, but

$$\begin{aligned}
 b &= \langle \hat{\mathbf{n}} \cdot \mathbf{v}, \hat{\mathbf{n}} \cdot \mathbf{v} \rangle_{\Gamma}, \\
 d &= \langle \hat{\mathbf{n}} \times \mathbf{w}, \hat{\mathbf{n}} \times \mathbf{w} \rangle_{\Gamma}, \\
 \tilde{b} &= \frac{1}{N_H} \sum_{i=1}^{N_2} \langle \hat{\mathbf{n}}_{2,i} \times \mathbf{v}, \hat{\mathbf{n}}_{2,i} \times \mathbf{v} \rangle_{\Gamma_{2,i}} + \frac{1}{N_H} \sum_{i=1}^{N_4} \langle \hat{\mathbf{n}}_{4,i} \cdot \mathbf{v}, \hat{\mathbf{n}}_{4,i} \cdot \mathbf{v} \rangle_{\Gamma_{4,i}}, \\
 \tilde{d} &= \frac{1}{N_E} \sum_{i=1}^{N_1} \langle \hat{\mathbf{n}}_{1,i} \times \mathbf{w}, \hat{\mathbf{n}}_{1,i} \times \mathbf{w} \rangle_{\Gamma_{1,i}} + \frac{1}{N_E} \sum_{i=1}^{N_3} \langle \hat{\mathbf{n}}_{3,i} \cdot \mathbf{w}, \hat{\mathbf{n}}_{3,i} \cdot \mathbf{w} \rangle_{\Gamma_{3,i}}.
 \end{aligned}$$

One can notice that $b \geq 0$ and $d \geq 0$. However, since there are fictitious interfaces that are collinear and orthogonal to each plane defined by the axis of the coordinate system and for each fictitious interface condition, we have $\tilde{b} \neq 0$ and $\tilde{d} \neq 0$. Requiring the Hessian matrix to be positive definite, one finds the following conditions:

$$\ell_h a + c_p b + c_f \tilde{b} > 0, \tag{12}$$

$$(\ell_h a + c_p b + c_f \tilde{b})(\ell_h c + c_p d + c_f \tilde{d}) - (\ell_h e)^2 > 0. \tag{13}$$

Condition (12) is always satisfied and condition (13) leads to the following criterion

$$\tilde{c} > \frac{e^2 - a c}{\tilde{c} \tilde{b} \tilde{d}} - \frac{c_p (a d + b c)}{c_f \tilde{b} \tilde{d}} - \frac{a \tilde{d} + \tilde{b} c}{\tilde{b} \tilde{d}} - \frac{c_p (b \tilde{d} + \tilde{b} d)}{\ell_h \tilde{b} \tilde{d}} - \frac{c_p^2 b d}{\ell_h c_f \tilde{b} \tilde{d}}, \tag{14}$$

where $\tilde{c} = \frac{c_f}{\ell_h}$. For a sufficiently large \tilde{c} , criterion (14) is satisfied. □

Let us now investigate the impact of the CFM based on minimization problem (11) on the stability of the original FD scheme. As shown previously, we have a system of the form (8) with \mathbf{D} coming from problem (11). However, this is not completely accurate since fictitious interface conditions (9) depend on FD solutions in Ω^+ . Computing Gateaux derivatives and using a necessary condition to obtain a minimum, we obtain

$$M \mathbf{c} = c_f \mathbf{b}_f + c_p \mathbf{b}_\Gamma,$$

where \mathbf{c} contains coefficients of polynomial approximations of the correction function, and \mathbf{b}_f and \mathbf{b}_Γ are associated with terms using respectively fictitious interfaces and embedded boundaries. Moreover, we can define a linear operator B that is such that $\mathbf{b}_f = B \mathbf{U}$. From Proposition 2, problem (11) is well-posed for appropriate fictitious interfaces, c_p and c_f , which leads to $\mathbf{c} = c_f M^{-1} B \mathbf{U} + c_p M^{-1} \mathbf{b}_\Gamma$. Hence, we have

$$\partial_t U(t) + L (I + c_f A M^{-1} B) \mathbf{U}(t) + c_p L A M^{-1} \mathbf{b}_\Gamma = 0,$$

where L is a finite difference operator, I is the identity operator and A is a linear operator that computes polynomial approximations of the correction function at nodes where it is needed. Since problem (11) is well-posed, we assume that the term $L A M^{-1} \mathbf{b}_\Gamma$ can be bounded. It is then sufficient to investigate the stability of

$$\partial_t U(t) + L (I + c_f A M^{-1} B) \mathbf{U}(t) = 0,$$

to identify any time-step criteria of the corresponding CFM-FDTD scheme [12]. We remark that we recover the original FDTD scheme in the limit when $c_f \rightarrow 0$ and therefore its properties. We therefore assume that we should be close to the stability condition of the

original FDTD scheme for a sufficient small c_f . This assumption is supported by numerical examples performed in Sect. 6.

In order to choose an appropriate penalization coefficient c_f , one should consider the following constraints. First, the priority should be given to embedded boundary conditions in problem (11), that is $c_p > c_f$. Second, the weight associated with fictitious interface conditions in the minimization problem should diminish as the length of local patches ℓ_h goes to zero, that is when the mesh grid size diminishes. This again enforces embedded boundary conditions and avoids any stability issues of CFM-FDTD schemes as the time-step size is refined. However, a too small value of c_f could lead to poorly conditioned matrices coming from the minimization problem (11).

3.2 Implementation of Fictitious Interface Conditions

This short subsection focuses on technical details concerning the implementation of fictitious interface conditions (9). Since Ω^- is a PEC domain, it is common to consider $\mathbf{H}^- = 0$ and $\mathbf{E}^- = 0$ as explained in Sect. 2. The natural extension of these electromagnetic fields in the non-PEC domain, that is Ω^+ , is then zero. Hence, $\mathbf{D}_H = \mathbf{H}^+$ and $\mathbf{D}_E = \mathbf{E}^+$. This allows us to enforce fictitious interface conditions in Ω^+ using finite difference approximations within it, namely $\mathbf{H}^* \approx \mathbf{H}^+$ and $\mathbf{E}^* \approx \mathbf{E}^+$.

Remark 1 In the case where \mathbf{H}^- is known and non-zero but still independent of time, one should also consider $\mathbf{D}_H = \mathbf{H}^+$, $\mathbf{D}_E = \mathbf{E}^+$, $\mathbf{H}^* \approx \mathbf{H}^+$ and $\mathbf{E}^* \approx \mathbf{E}^+$. However, the embedded boundary condition for the magnetic field becomes $\hat{\mathbf{n}} \cdot (\mu \mathbf{H}^+) = b(\mathbf{x})$, where $b(\mathbf{x}) = \hat{\mathbf{n}} \cdot (\mu \mathbf{H}^-(\mathbf{x}))$.

To ease the implementation of fictitious interface conditions (9), we choose fictitious interfaces that are aligned with the mesh grid. In other words, fictitious interfaces $\Gamma_{k,i}$ are chosen in such a way that their normal $\hat{\mathbf{n}}_{k,i}$ is an element of the standard basis in \mathbb{R}^3 . This facilitates the construction of space–time interpolating polynomials that use FD approximations. Let us consider the transverse magnetic (TM_z) mode (see Sect. 6), which is a 2-D simplification of Maxwell's equations, as an example. In this case, the normal of a fictitious interface is either $\mathbf{n}_1 = (1, 0)$ or $\mathbf{n}_2 = (0, 1)$. Hence, $\mathbf{n}_1 \cdot \mathbf{H}^* = H_x^*$, $\mathbf{n}_2 \cdot \mathbf{H}^* = H_y^*$, $\mathbf{n}_1 \times \mathbf{H}^* = H_y^* \mathbf{n}_2$, $\mathbf{n}_2 \times \mathbf{H}^* = -H_x^* \mathbf{n}_1$, $\mathbf{n}_1 \times \mathbf{E}^* = (0, -E_z^*)$ and $\mathbf{n}_2 \times \mathbf{E}^* = (E_z^*, 0)$. Figure 2 illustrates fictitious interfaces that can be generated for a given local patch and a staggered grid that is described in Sect. 6.1.

The functional (10) involves time integrals of finite difference approximations \mathbf{H}^* and \mathbf{E}^* in the vicinity of the boundary Γ . Since the time interval associated with local patches is given by $I_\Gamma^h = [t_n - \Delta t_\Gamma, t_n]$, we can use previous computed finite difference solutions to construct the space–time interpolant needed for fictitious interface conditions. However, this makes difficult the initialization of a CFM-FDTD scheme that uses fictitious interfaces. In Sects. 4 and 5, we propose an initialization strategy for the Yee scheme and a fourth-order FDTD scheme.

3.3 Computation of Local Patches

The computation of an appropriate local patch Ω_Γ^h is essential for the CFM. The well-posedness of problem (3) and (11) highly depends on the representation of the embedded boundary within the local patch Ω_Γ^h . Hence, an appropriate local patch is of foremost importance to obtain an accurate approximation of a correction function. In previous CFM-FDTD

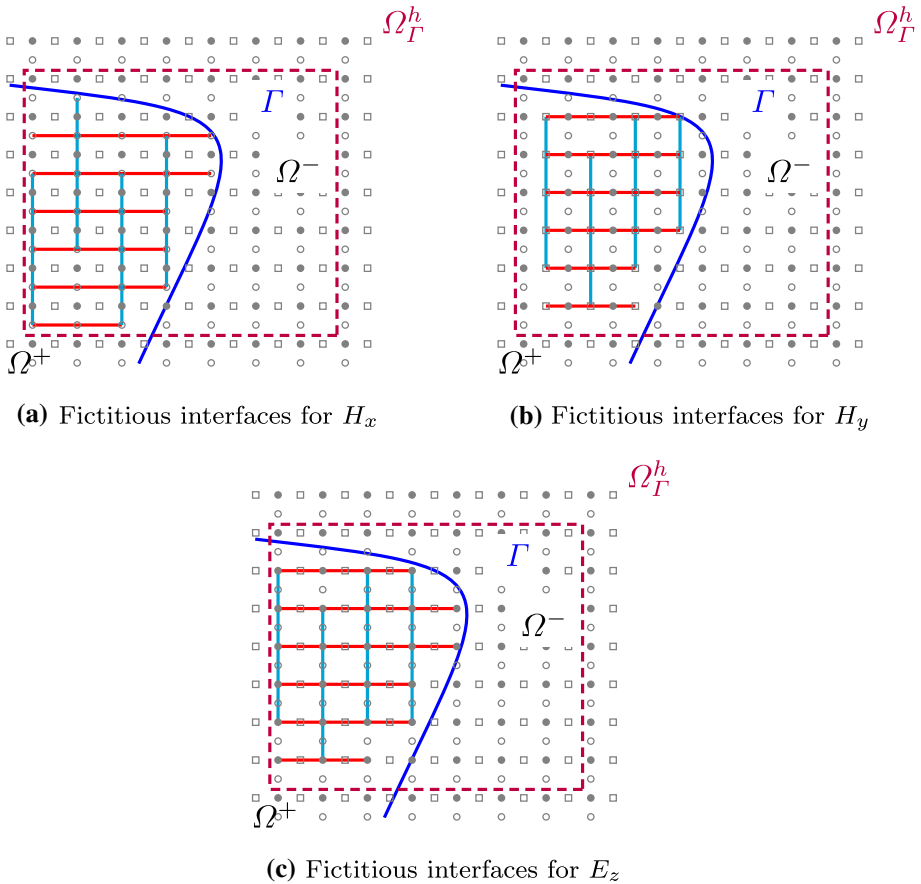


Fig. 2 An example of a local patch Ω_Γ^h with fictitious interfaces. The x -component and the y -component of the magnetic field are respectively represented by \circ and \square while the z -component of the electric field is represented by \bullet . Fictitious interfaces associated with $\mathbf{n}_1 = (1, 0)$ and $\mathbf{n}_2 = (0, 1)$ are respectively represented by — and —

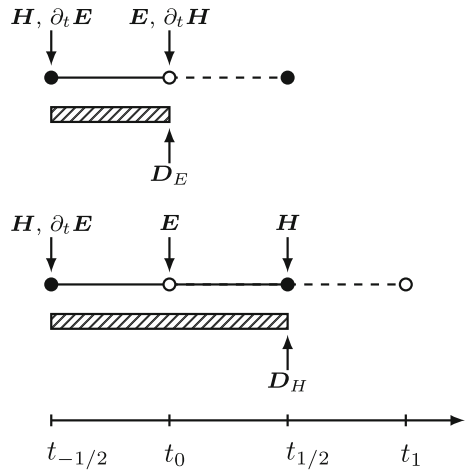
schemes, a “Node Centered” approach is used to compute local patches [19,20]. This approach consists to define a local patch and solve a minimization problem for each node to be corrected. Even though it is more expensive than other constructions of local patches, “Node Centered” approaches have the benefit to guarantee the uniqueness of the correction function at a given node. Hence, a common discrete measure of the divergence for staggered FDTD schemes is conserved for some nodes close to the embedded boundary [19].

In this work, as it is done for other immersed boundary methods [18,23], we directly discretize the embedded boundary. Let us now summarize this approach. For simplicity, let us consider $\Omega \subset \mathbb{R}^2$. Assume a given embedded boundary Γ that can be parametrized with respect to the parameter $s \in [s_a, s_b]$. The number of local patches is given by

$$N_s \approx \frac{L_\Gamma}{\alpha h} + 1, \tag{15}$$

where L_Γ is the estimated arc length of Γ , h is the mesh grid size and α is a positive constant. In this work, we use $\alpha = 2$. Hence, centre points of local patches are given by

Fig. 3 Initialization strategy for the proposed CFM-Yee scheme. The black and white circle marker represent respectively the magnetic field and the electric field. The dashed box illustrates the time interval I_Γ^h of local patches



$\mathbf{x}_{c,i} = (x(s_i), y(s_i))$, where $s_i = s_a + i \Delta s$ for $i = 0, \dots, N_s - 1$ and $\Delta s = \frac{s_b - s_a}{N_s - 1}$. For a given node to be corrected at \mathbf{x}_D , we find the closest $\mathbf{x}_{c,i}$ and associate the corresponding local patch to \mathbf{x}_D . We therefore guarantee the uniqueness of the correction function to each node to be corrected while reducing the computational cost, particularly for large stencils, when compared with “Node Centered” approaches. The local patches are square and aligned with the computational grid. The length in space of local patches is $\ell_h = \beta h$, where h is the mesh grid size and β is a positive constant. It is worth mentioning that the parameter β is chosen in such a way that enough fictitious interfaces can be generated within Ω_Γ^h and that all nodes to be corrected are associated with a local patch. As for the time interval $I_\Gamma^h = [t_n - \Delta t_\Gamma, t_n]$, we choose Δt_Γ in such a way that I_Γ^h includes the number of time steps needed to construct space–time interpolants associated with fictitious interface conditions.

4 Application of the CFM to the Yee Scheme

In this section, we apply the CFM to the well-known Yee scheme [27], which is a popular FDTD scheme in computational electromagnetics, with a particular attention on its initialization. Let us recall that the Yee scheme uses a staggered grid in both space and time. We then need to adapt the functional (10), and more precisely the interval of integration in time of fictitious interface conditions, in order to consider a staggered grid in time. Finally, we conclude with pros and cons of such an approach. In the following, we assume that the parameter β has been chosen in such a way that enough fictitious interfaces have been generated within Ω_Γ^h (see Sect. 3.3) and we therefore focus on the time component.

Let us first define a staggered grid in time. We consider a time interval $I = [0, T]$ subdivided into N_t subintervals of length Δt . We then have $t_n := n \Delta t$ for $n = 0, \dots, N_t$ and $t_{n+1/2} := (n + 1/2) \Delta t$ for $n = -1, \dots, N_t - 1$. The magnetic and electric fields are respectively defined at $t_{n+1/2}$ and t_n .

According to the Yee scheme, we first compute $\mathbf{H}^{1/2}$ using initial conditions $\mathbf{H}^{-1/2}$ and \mathbf{E}^0 , as illustrated in Fig. 3. In this case, the CFM-Yee scheme needs to provide corrections for the electric field at t_0 , that is \mathbf{D}_E^0 . The time interval of local patches is then $I_\Gamma^h = [t_{-1/2}, t_0]$. At first sight, we do not have enough information in time within local patches to build space–time interpolants that are accurate enough for fictitious interface conditions. However, by

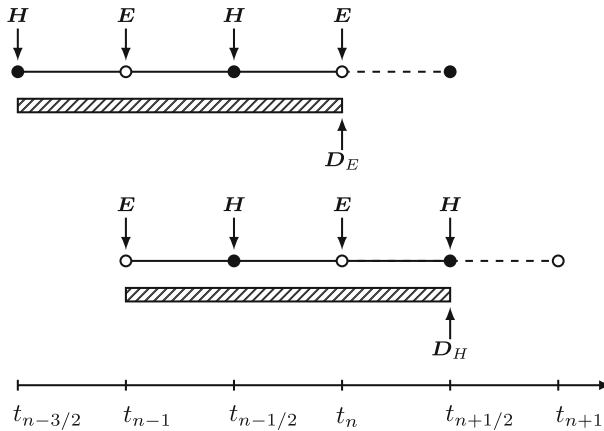


Fig. 4 Strategy for a CFM-Yee scheme. The black and white circle marker represent respectively the magnetic field and the electric field. The dashed box illustrates the time interval I_{Γ}^h of local patches

Faraday’s law (1a) and Ampère–Maxwell’s law (1b), we have $\partial_t \mathbf{H}^+ = -\mu^{-1} \nabla \times \mathbf{E}^+$ and $\partial_t \mathbf{E}^+ = \epsilon^{-1} \nabla \times \mathbf{H}^+$ in Ω^+ . We can then compute the first-order time derivative of \mathbf{H} at t_0 and \mathbf{E} at $t_{-1/2}$ using the curl of \mathbf{E}^0 and $\mathbf{H}^{-1/2}$. It is worth mentioning that one could estimate the curl operator using appropriate finite difference approximations. First-degree polynomials in time can be constructed using $\mathbf{H}^{-1/2}$ and $\partial_t \mathbf{H}^0$, and \mathbf{E}^0 and $\partial_t \mathbf{E}^{-1/2}$. Hence, the interval of integration in time associated with all fictitious interface conditions in functional (10) is also I_{Γ}^h .

For the computation of \mathbf{E}^1 , one needs correction functions for the magnetic field at $t_{1/2}$, that is $\mathbf{D}_H^{1/2}$, as illustrated in Fig. 3. The time interval of local patches is then $I_{\Gamma}^h = [t_{-1/2}, t_{1/2}]$. In this situation, we construct a first-degree polynomial in time for the electric field using again \mathbf{E}^0 and $\partial_t \mathbf{E}^{-1/2}$. As for the magnetic field, we use $\mathbf{H}^{-1/2}$ and $\mathbf{H}^{1/2}$ to compute a first-degree polynomial in time. The interval of integration in time associated with fictitious interface conditions involving the magnetic field is then $[t_{-1/2}, t_{1/2}]$ while the one associated with the electric field is $[t_{-1/2}, t_0]$.

Once the initialization of the proposed CFM-Yee scheme is done, we only have two cases to consider, as illustrated in Fig. 4. The first case involves the computation of $\mathbf{H}^{n+1/2}$ and therefore \mathbf{D}_E^n . The time interval of local patches is $I_{\Gamma}^h = [t_{n-3/2}, t_n]$. Approximations of the magnetic field at $t_{n-3/2}$ and $t_{n-1/2}$ are used to construct a first-degree polynomial interpolant in time. This leads to an interval of integration in time associated with fictitious interface conditions involving the magnetic field of $[t_{n-3/2}, t_{n-1/2}]$. As for fictitious interface conditions of the electric field, the interval of integration in time is $[t_{n-1}, t_n]$, and \mathbf{E}^{n-1} and \mathbf{E}^n are used to construct a first-degree polynomial in time. The second case implies the computation of \mathbf{E}^{n+1} . We then need to compute $\mathbf{D}_H^{n+1/2}$ and therefore $I_{\Gamma}^h = [t_{n-1}, t_{n+1/2}]$. First-degree polynomials in time are constructed using $\mathbf{H}^{n-1/2}$ and $\mathbf{H}^{n+1/2}$, and \mathbf{E}^{n-1} and \mathbf{E}^n . This leads to intervals of integration in time of fictitious interfaces given by $[t_{n-1/2}, t_{n+1/2}]$ for the magnetic field and $[t_{n-1}, t_n]$ for the electric field.

Another avenue to initialize the proposed CFM-Yee scheme, although it is very specific to some applications, is to consider that \mathbf{H}^+ and \mathbf{E}^+ in the vicinity of the embedded boundary remain unchanged for $t \leq t_0$. Hence, the numerical strategy described previously for Fig. 4 can be directly used. As an example, this approach could be useful for scattering problems.

Finally, the main disadvantage of this approach is the computation cost associated with minimization problems of the CFM at each update of electromagnetic fields. In fact, the CFM consumes most of the computational time when compared with the finite-difference part. However, a parallel implementation of the computation of approximations of the correction function can be performed since minimization problems associated with local patches are independent at a given time step. We refer to [1] for more details about the benefits of a parallel implementation of the CFM. It is also worth mentioning that we do not have to keep the whole previous solutions but only approximations associated with fictitious interfaces. Despite this drawback, the proposed CFM-Yee scheme could achieve second-order convergence for appropriate approximations of the correction function (see Proposition 3) while treating various complex geometries of the embedded boundary without significantly increasing the complexity of the numerical approach. Moreover, it can also be implemented as a black-box for existing softwares that use the Yee scheme.

5 Application of the CFM on a Fourth-Order Staggered FDTD Scheme

In this section, we introduce a CFM-FDTD scheme based on a fourth-order staggered FDTD scheme. The staggered space and time grids are defined as in the Yee scheme. Spatial derivatives are estimated using the fourth-order centered approximation. As for time derivatives, many avenues can be chosen, such as staggered Adams–Bashforth or staggered backward differentiation methods [11]. In this work, we choose a fourth-order staggered free-parameter multistep method introduced in [11], which has a maximum imaginary stability boundary close to the leapfrog method used in the Yee scheme.

In the following, we first describe a fourth-order staggered free-parameter multistep method that is used to discretize time derivatives. We assume that previous solutions needed for the initialization of the multistep method are given. Afterward, we introduce the associated CFM-FDTD scheme with a particular attention on the time component. As in Sect. 4, we assume that the parameter β has been chosen in such a way that enough fictitious interfaces have been generated within Ω_R^h .

Let us consider $\partial_t \mathbf{H} = \mathbf{f}_H(\mathbf{E})$ and $\partial_t \mathbf{E} = \mathbf{f}_E(\mathbf{H})$. The considered fourth-order free-parameter method is given by

$$\begin{aligned}
 \mathbf{H}^{n+1/2} &= -\alpha_3 \mathbf{H}^{n-1/2} - \alpha_2 \mathbf{H}^{n-3/2} - \alpha_1 \mathbf{H}^{n-5/2} - \alpha_0 \mathbf{H}^{n-7/2} \\
 &\quad + \Delta t (\beta_3 \mathbf{f}_H(\mathbf{E}^n) + \beta_2 \mathbf{f}_H(\mathbf{E}^{n-1}) + \beta_1 \mathbf{f}_H(\mathbf{E}^{n-2})) \\
 \mathbf{E}^{n+1} &= -\alpha_3 \mathbf{E}^n - \alpha_2 \mathbf{E}^{n-1} - \alpha_1 \mathbf{E}^{n-2} - \alpha_0 \mathbf{E}^{n-3} \\
 &\quad + \Delta t (\beta_3 \mathbf{f}_E(\mathbf{H}^{n+1/2}) + \beta_2 \mathbf{f}_E(\mathbf{H}^{n-1/2}) + \beta_1 \mathbf{f}_E(\mathbf{H}^{n-3/2}))
 \end{aligned} \tag{16}$$

where $\beta_1 = t, \beta_2 = s, \beta_3 = \frac{1}{22} s + \frac{12}{11}$,

$$\begin{aligned}
 \alpha_0 &= -\frac{1}{22} - \frac{1}{528} s + \frac{1}{24} t, \\
 \alpha_1 &= \frac{5}{22} + \frac{9}{176} s - \frac{9}{8} t, \\
 \alpha_2 &= -\frac{9}{22} - \frac{201}{176} s + \frac{9}{8} t, \\
 \alpha_3 &= -\frac{17}{22} + \frac{577}{528} s - \frac{1}{24} t
 \end{aligned}$$

with $s = -1$ and $t = 1.045$.

Let us now introduce the corresponding CFM-FDTD scheme. The time scheme (16) needs to compute $\mathbf{f}_H(\mathbf{E})$ at t_n, t_{n-1} and t_{n-2} , and $\mathbf{f}_E(\mathbf{H})$ at $t_{n+1/2}, t_{n-1/2}$ and $t_{n-3/2}$. Hence, we need to keep previous corresponding correction functions. For the computation of $\mathbf{H}^{n+1/2}$, we set $I_\Gamma^h = [t_{n-7/2}, t_n]$ and compute \mathbf{D}_E^n . It is worth mentioning that, at the first update of the magnetic field to estimate $\mathbf{H}^{1/2}$, we compute the correction function \mathbf{D}_E at t_0, t_{-1} and t_{-2} , and \mathbf{D}_H at $t_{-1/2}$ and $t_{-3/2}$. For the update of the electric field, that is \mathbf{E}^{n+1} , we set $I_\Gamma^h = [t_{n-3}, t_{n+1/2}]$ and compute $\mathbf{D}_H^{n+1/2}$. As for the Yee scheme, we need to adapt the interval of integration in time of fictitious interface conditions using a similar procedure as in Sect. 4 for both cases.

6 Transverse Magnetic Mode Numerical Examples

Let us consider the transverse magnetic (TM_z) mode. The unknowns are $H_x(x, y, t)$, $H_y(x, y, t)$ and $E_z(x, y, t)$. For a domain $\Omega \subset \mathbb{R}^2$ and constant physical parameters, Maxwell’s equations are then simplified to

$$\begin{aligned} \mu \partial_t H_x + \partial_y E_z &= 0 \quad \text{in } \Omega \times I, \\ \mu \partial_t H_y - \partial_x E_z &= 0 \quad \text{in } \Omega \times I, \\ \epsilon \partial_t E_z - \partial_x H_y + \partial_y H_x &= 0 \quad \text{in } \Omega \times I, \\ \partial_x H_x + \partial_y H_y &= 0 \quad \text{in } \Omega \times I \end{aligned} \tag{17}$$

with the associated boundary, initial conditions and

$$\begin{aligned} \hat{n}_x H_x^+ + \hat{n}_y H_y^+ &= 0 \quad \text{on } \Gamma \times I, \\ E_z^+ &= 0 \quad \text{on } \Gamma \times I, \end{aligned} \tag{18}$$

as embedded boundary conditions for Ω^+ .

In the following, we name the CFM-FDTD scheme based on the Yee scheme as CFM-Yee scheme while the one based on a fourth-order staggered FDTD scheme is named CFM-4th scheme. The error of $\mathbf{U} = [H_x, H_y, E_z]^T$ at t_n is computed using approximations and analytic solutions of the magnetic field and the electric field at respectively $t_n - \frac{\Delta t}{2}$ and t_n because of the staggered grid in time.

6.1 A 2-D Staggered Space Discretization

In this subsection, we present a staggered grid in space. Let us consider a rectangular domain $\Omega = [x_\ell, x_r] \times [y_b, y_t] \subset \mathbb{R}^2$. The domain is divided in $N = N_x N_y$ square cells, noted by $\Omega_{ij} = [x_{i-1/2}, x_{i+1/2}] \times [y_{j-1/2}, y_{j+1/2}]$ and centered at

$$(x_i, y_j) = (x_\ell + (i - \frac{1}{2}) \Delta x, y_b + (j - \frac{1}{2}) \Delta y)$$

for $i = 1, \dots, N_x$ and $j = 1, \dots, N_y$ with $\Delta x := (x_r - x_\ell)/N_x$ and $\Delta y := (y_t - y_b)/N_y$. The z -component of the electric field is approximated at the center of the cell. The x -component and y -component of the magnetic field are respectively approximated at

$$(x_i, y_{j+1/2}) = (x_\ell + (i - \frac{1}{2}) \Delta x, y_b + j \Delta y)$$

for $i = 1, \dots, N_x$ and for $j = 0, \dots, N_y$, and

$$(x_{i+1/2}, y_j) = (x_\ell + i \Delta x, y_b + (j - \frac{1}{2}) \Delta y)$$

for $i = 0, \dots, N_x$ and for $j = 1, \dots, N_y$. We use either the second or fourth order centered finite difference scheme in space. As an example, the x -derivative of H_y is of the form

$$\partial_x H_y(x_i, y_j, t_{n+1/2}) \approx \frac{H_{y,i+1/2,j}^{n+1/2} - H_{y,i-1/2,j}^{n+1/2}}{\Delta x}$$

and

$$\partial_x H_y(x_i, y_j, t_{n+1/2}) \approx \frac{H_{y,i-3/2,j}^{n+1/2} - 27 H_{y,i-1/2,j}^{n+1/2} + 27 H_{y,i+1/2,j}^{n+1/2} - H_{y,i+3/2,j}^{n+1/2}}{24 \Delta x}$$

for respectively the second and fourth order centered finite-difference. Finally, as it is commonly used, we impose $E_z = 0$ and $H_x = H_y = 0$ in PEC subdomains.

6.2 Problems with an Analytic Solution

In this subsection, we perform numerical examples with analytic solutions to assess the impact of the penalization coefficient c_f and to verify the proposed numerical approach. The domain Ω is divided into two subdomains Ω^+ and Ω^- . Periodic boundary conditions are used on all $\partial\Omega$. We set $c_p = 1$. The mesh grid size is such that $h = \Delta x = \Delta y$. We use second and third degree polynomial approximations of the correction function for respectively the CFM-Yee scheme and the CFM-4th scheme. Hence, this should lead to a second and third order convergence in L^2 -norm (see Proposition 3). We set $\ell_h = 7h$, and we construct \mathbf{E}^* and \mathbf{H}^* in Ω^+ using at least a second degree interpolating polynomial in space for both schemes.

6.2.1 Circular Cavity Problem

Let us consider a holed PEC material. The domain is $\Omega = [-1.25, 1.25] \times [-1.25, 1.25]$. Since Ω^- is a PEC subdomain, the embedded boundary Γ then encloses subdomain Ω^+ . The embedded boundary is a circle centered at $(0, 0)$ with unit radius. The physical parameters are $\epsilon = 1$ and $\mu = 1$. The time-step size is $\Delta t = \frac{h}{2}$ for both CFM-FDTD schemes. In subdomain Ω^+ , the solution in cylindrical coordinates is given by

$$\begin{aligned} H_\rho^+(\rho, \phi, t) &= \frac{i}{\alpha_{i,j} \rho} J_i(\alpha_{i,j} \rho) \sin(i \phi) \sin(\alpha_{i,j} t), \\ H_\phi^+(\rho, \phi, t) &= \frac{1}{2} (J_{i-1}(\alpha_{i,j} \rho) - J_{i+1}(\alpha_{i,j} \rho)) \cos(i \phi) \sin(\alpha_{i,j} t), \\ E_z^+(\rho, \phi, t) &= J_i(\alpha_{i,j} \rho) \cos(i \phi) \cos(\alpha_{i,j} t), \end{aligned}$$

where $\alpha_{i,j}$ is the j -th positive real root of the i -order Bessel function of first kind J_i . In this numerical example, we choose $i = 6$ and $j = 2$.

Let us assess the impact of the penalization coefficient c_f on the proposed CFM-FDTD schemes. Fig. 5 illustrates convergence plots of $\mathbf{U} = [H_x, H_y, E_z]^T$ in L^2 -norm for both CFM-FDTD schemes using different values of c_f , that is Δt , $\frac{\Delta t}{2}$ and $\frac{\Delta t}{4}$. The time interval is $I = [0, 0.5]$. We observe a clear second-order convergence for the CFM-Yee scheme. For the CFM-4th scheme, a fourth-order convergence is observed, which is better than expected. The

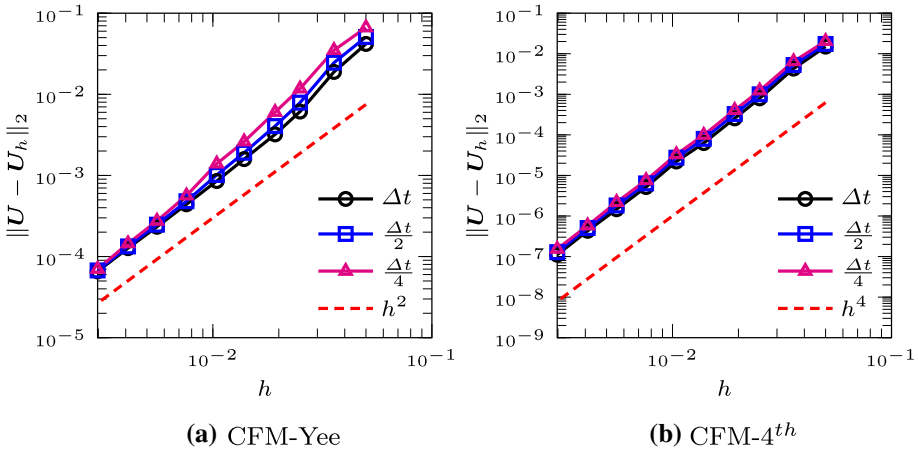


Fig. 5 Convergence plots in L^2 -norm for a TM_z mode circular cavity problem using the proposed CFM-FDTD schemes for different values of c_f , that is Δt , $\frac{\Delta t}{2}$ and $\frac{\Delta t}{4}$

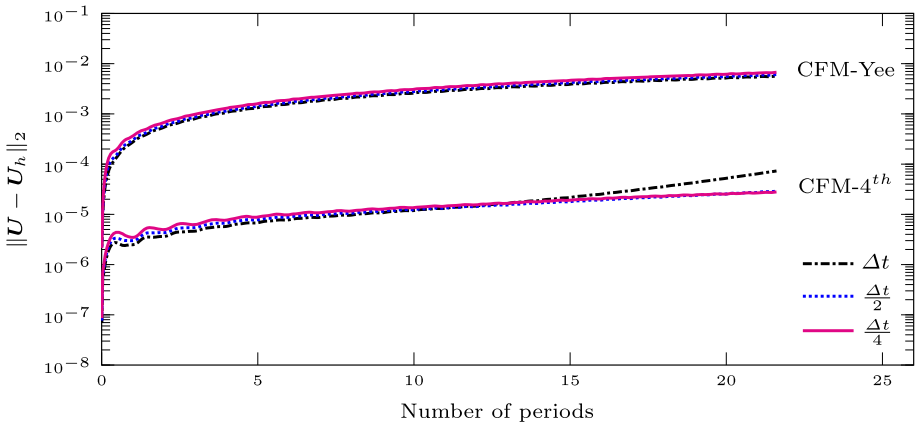


Fig. 6 Evolution in time of the error of U in L^2 -norm for a TM_z mode circular cavity problem using CFM-FDTD schemes with $h = \frac{1}{160}$ and different values of c_f , that is Δt , $\frac{\Delta t}{2}$ and $\frac{\Delta t}{4}$

obtained convergence orders are in agreement with the theory for all values of c_f . However, one can notice that the error slightly increases as the value of c_f diminishes. Let us now perform long time simulations. Figure 6 illustrates the evolution of the error of electromagnetic fields in L^2 -norm as a function of the number of periods for different values of c_f . The time interval is $I = [0, 10]$ and the mesh grid size is $h = \frac{1}{160}$. Numerical results suggest that the CFM-Yee scheme is stable for the considered values of the penalization coefficient c_f . However, the CFM-4th scheme seems more sensitive than the CFM-Yee scheme to the value of c_f . Stability issues appear after a dozen periods for the largest considered value of the penalization coefficient, that is $c_f = \Delta t$. The penalization coefficient c_f must be therefore chosen small enough to avoid stability problems as the mesh grid size diminishes. Based on these numerical results, we choose $c_f = \Delta t$ and $c_f = \frac{\Delta t}{4}$ for respectively the CFM-Yee scheme and the CFM-4th scheme to avoid any stability issues in all other numerical examples.

Fig. 7 Convergence plots in L^2 -norm for a TM_z mode square cavity problem using the proposed CFM-FDTD schemes

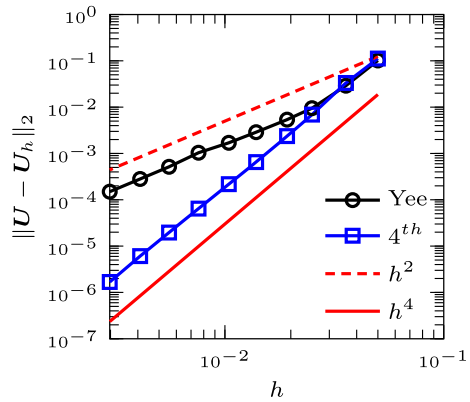
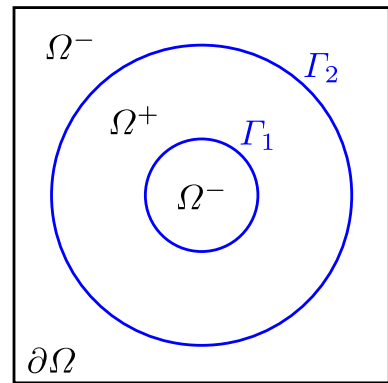


Fig. 8 Geometry of a two concentric PEC cylinders problem



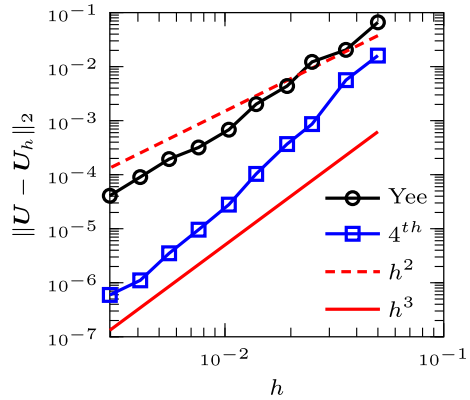
6.2.2 Square Cavity Problem

Let us consider a PEC material with square holes. The domain is $\Omega = [-0.75, 0.75] \times [-0.75, 0.75]$ and the time interval is $I = [0, 0.5]$. Since Ω^- is a PEC subdomain, the boundary Γ then encloses subdomain Ω^+ . The boundary Γ is a square of unit length centered at $(0, 0)$. The physical parameters are $\epsilon = 1$ and $\mu = 1$. The time-step size is $\Delta t = \frac{h}{2}$ for both CFM-FDTD schemes. In Ω^+ , the solution is given by

$$\begin{aligned}
 H_x^+(x, y, t) &= -\frac{\pi n}{\omega} \sin(m \pi x) \cos(n \pi y) \sin(\omega t), \\
 H_y^+(x, y, t) &= \frac{\pi m}{\omega} \cos(m \pi x) \sin(n \pi y) \sin(\omega t), \\
 E_z^+(x, y, t) &= \sin(m \pi x) \cos(n \pi y) \cos(\omega t),
 \end{aligned}$$

where $\omega = \pi \sqrt{m^2 + n^2}$ with $m, n > 0$ [15]. In this numerical example, we choose $m = n = 4$. Convergence plots are illustrated in Fig. 7 for both proposed CFM-FDTD schemes. A second and fourth order convergence are observed for respectively the CFM-Yee scheme and the fourth-order CFM-FDTD scheme in L^2 -norm. The obtained convergence orders are in agreement with the theory.

Fig. 9 Convergence plots in L^2 -norm for a TM_z mode two concentric PEC cylinders problem using the proposed CFM-FDTD schemes



6.2.3 Two Concentric PEC Cylinders Problem

This problem considers a holed PEC containing a PEC cylinder as illustrated in Fig. 8. It is recalled that Ω^- is a PEC subdomain. We therefore have subdomain Ω^+ enclosed by two PEC walls on Γ_1 and Γ_2 . There are two circular embedded boundaries centered at $(0, 0)$ with radius $r_1 = \frac{1}{3}$ and $r_2 = 1$ for respectively Γ_1 and Γ_2 . The domain is $\Omega = [-1.25, 1.25] \times [-1.25, 1.25]$ and the time interval is $I = [0, 0.75]$. The physical parameters are $\epsilon = \frac{1}{2}$ and $\mu = \frac{1}{2}$. The time-step size is $\Delta t = \frac{h}{4}$ for both CFM-FDTD schemes. In subdomain Ω^+ , the solution in cylindrical coordinates is given by

$$\begin{aligned}
 H_x^+(\rho, \phi, t) &= -\frac{1}{2} \sin(\omega t + \phi) \sin(\phi) \left(J_0\left(\frac{\omega\rho}{2}\right) - J_2\left(\frac{\omega\rho}{2}\right) + \alpha Y_0\left(\frac{\omega\rho}{2}\right) - \alpha Y_2\left(\frac{\omega\rho}{2}\right) \right) \\
 &\quad - \frac{2 \cos(\phi)}{\omega \rho} \cos(\omega t + \phi) \left(J_1\left(\frac{\omega\rho}{2}\right) + \alpha Y_1\left(\frac{\omega\rho}{2}\right) \right), \\
 H_y^+(\rho, \phi, t) &= \frac{1}{2} \sin(\omega t + \phi) \cos(\phi) \left(J_0\left(\frac{\omega\rho}{2}\right) - J_2\left(\frac{\omega\rho}{2}\right) + \alpha Y_0\left(\frac{\omega\rho}{2}\right) - \alpha Y_2\left(\frac{\omega\rho}{2}\right) \right) \\
 &\quad - \frac{2 \sin(\phi)}{\omega \rho} \cos(\omega t + \phi) \left(J_1\left(\frac{\omega\rho}{2}\right) + \alpha Y_1\left(\frac{\omega\rho}{2}\right) \right), \\
 H_z^+(\rho, \phi, t) &= \cos(\omega t + \phi) \left(J_1\left(\frac{\omega\rho}{2}\right) + \alpha Y_1\left(\frac{\omega\rho}{2}\right) \right),
 \end{aligned}$$

where $\alpha \approx 1.76368380110927$, $\omega \approx 9.813695999428405$, and J_i and Y_i are the i -order Bessel function of respectively first and second kind [8]. Convergence plots are illustrated in Fig. 9 for both proposed CFM-FDTD schemes. As expected, we observe a second and third order convergence for respectively the CFM-Yee scheme and the CFM-4th scheme in L^2 -norm.

6.3 Problems with a Manufactured Solution

Let us now consider more complex embedded boundaries. To our knowledge, there is no analytical solution for Maxwell’s equations with arbitrary embedded boundaries. We therefore consider that embedded boundary conditions are given by

$$\begin{aligned}
 \hat{n} \times \mathbf{E}^+ &= \mathbf{a}(\mathbf{x}, t) \quad \text{on } \Gamma \times I, \\
 \hat{n} \cdot (\mu \mathbf{H}^+) &= \mathbf{b}(\mathbf{x}, t) \quad \text{on } \Gamma \times I,
 \end{aligned} \tag{19}$$

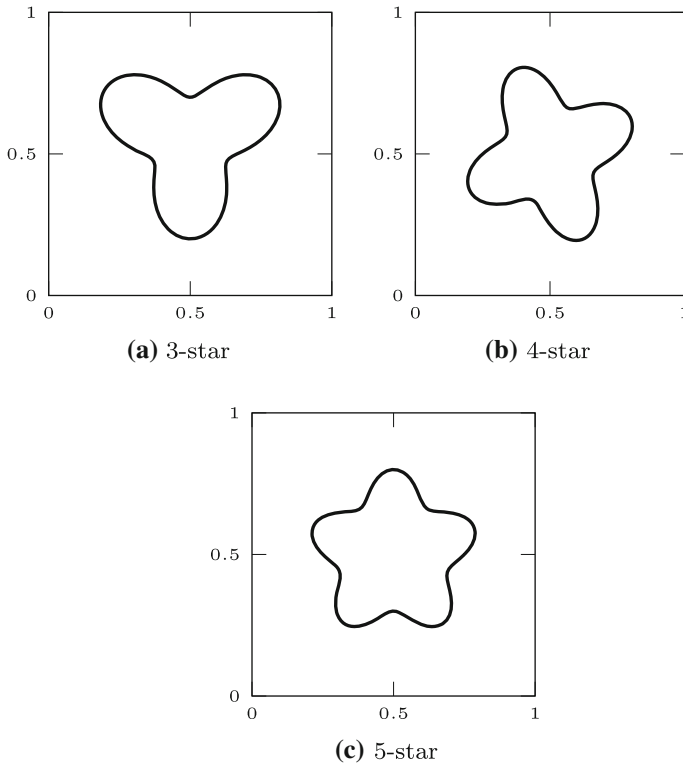
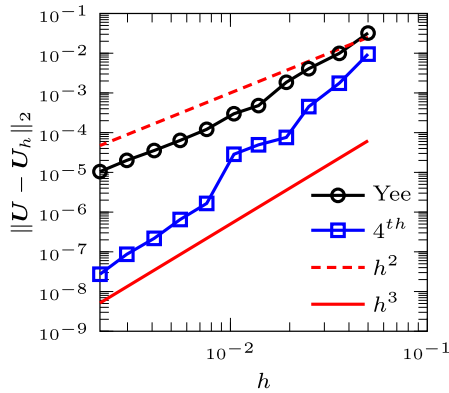


Fig. 10 Different geometries of an embedded PEC

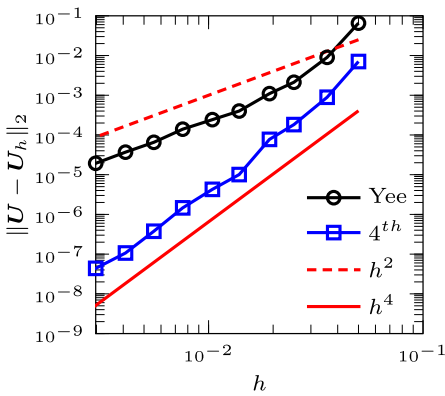
where $\mathbf{a}(\mathbf{x}, t)$ and $\mathbf{b}(\mathbf{x}, t)$ are known functions. The physical parameters are $\epsilon = 1$ and $\mu = 2$. The time-step size is $\Delta t = \frac{h}{2}$ for both CFM-FDTD schemes. We also consider the 3-star, 4-star and 5-star embedded boundaries illustrated in Fig. 10. The solutions are

$$\begin{aligned} H_x^+ &= 0.5 \sin(2\pi x) \sin(2\pi y) \sin(2\pi t), \\ H_y^+ &= 0.5 \cos(2\pi x) \cos(2\pi y) \sin(2\pi t), \\ E_z^+ &= \sin(2\pi x) \cos(2\pi y) \cos(2\pi t) \end{aligned}$$

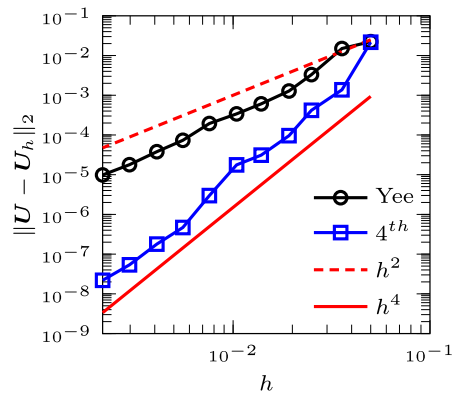
in Ω^+ while $H_x^- = H_y^- = 0$ and $E_z^- = 0$ in Ω^- . Since functions \mathbf{a} and \mathbf{b} depend on \mathbf{x} and t , boundary conditions (19) will differ depending on the geometry of the embedded boundary. It is worth noting that manufactured solutions are at divergence-free in each subdomain, but not in the whole domain because of embedded boundary conditions that we impose. Nevertheless, this allows us to assess the performance of the proposed CFM-FDTD schemes in a more general framework. The time interval is $I = [0, 1]$. We set $\ell_h = 6h$ for the 4-star embedded boundary while $\ell_h = 7h$ for the 3-star and 5-star embedded boundaries. The other parameters are the same as problems with analytical solutions in Sect. 6.2. Convergence plots for each geometry of the embedded boundary are illustrated in Fig. 11 using both proposed CFM-FDTD schemes. For all embedded boundaries, we observe a clear second-order convergence for the CFM-Yee scheme. As for the CFM-4th scheme, we observe a third-order convergence for the 3-star boundary while a fourth-order convergence is obtained for the 4-star and 5-star boundaries.



(a) 3-star



(b) 4-star



(c) 5-star

Fig. 11 Convergence plots in L^2 -norm for TM_z mode problems with a manufactured solution using the proposed CFM-FDTD schemes and different geometries of the embedded boundary

6.4 Scattering Problems

Let us now consider scattering problems involving various geometries of a PEC. To our knowledge, there is no analytic solution for these problems with arbitrary geometries of the embedded boundary. Hence, we estimate errors using approximate solutions coming from a very fine mesh grid. The reference solution U^* is computed using $h = \frac{1}{1620}$ and the CFM-4th scheme. All nodes used for H and E in coarser grids with $h \in \{\frac{1}{20}, \frac{1}{60}, \frac{1}{180}, \frac{1}{540}\}$ are also part of the finest grid. The domain is $\Omega = [-1, 1.5] \times [-0.75, 1.75]$ and the time interval is $I = [0, 1.5]$. Periodic conditions are used on all $\partial\Omega$. We consider the 3-star and 5-star embedded boundaries, and a circular PEC centered at $(0.5, 0.5)$ with a radius of $r = 0.25$. The physical parameters are $\epsilon = 1$ and $\mu = 1$. The mesh grid size is $h = \Delta x = \Delta y$. The time-step size is $\Delta t = \frac{h}{2}$. The length of local patches is $\ell_h = 6h$ for the circular PEC, and $\ell_h = 7h$ for the 5-star PEC and 3-star PEC. The other parameters are the same as problems with analytical solutions in Sect. 6.2.

Let us consider a pulsed wave propagating in the positive x -direction, given by

$$\begin{aligned} H_{x_p}(\mathbf{x}, t) &= 0, \\ H_{y_p}(\mathbf{x}, t) &= -\frac{2}{\sigma^2} (x - \gamma - t) e^{-\left(\frac{x-\gamma-t}{\sigma}\right)^2}, \\ E_{z_p}(\mathbf{x}, t) &= \frac{2}{\sigma^2} (x - \gamma - t) e^{-\left(\frac{x-\gamma-t}{\sigma}\right)^2}, \end{aligned} \tag{20}$$

where $\sigma = 0.1$ and $\gamma = -0.3$. It is worth mentioning that we use electromagnetic fields given in (20) to compute all previous solutions needed to initialize the time-stepping method presented in Sect. 5. It is recalled that we set $H_x^- = H_y^- = 0$ and $E_z^- = 0$ in the PEC subdomain, that is Ω^- . Figure 12 illustrates convergence plots for each geometry of the embedded PEC using both CFM-FDTD schemes. We observe a second and fourth order convergence for respectively the CFM-Yee scheme and the CFM-4th scheme. Figures 13, 14 and 15 illustrate the evolution of the magnitude of each component of electromagnetic fields. The numerical approach can handle various geometries of the embedded boundary without significantly increasing the complexity of the method.

7 A Remark on the Transverse Electric Mode

For the transverse electric (TE_z) mode, the unknowns are $E_x(x, y, t)$, $E_y(x, y, t)$ and $H_z(x, y, t)$, and the system of equations are given by

$$\begin{aligned} \mu \partial_t H_z - \partial_y E_x + \partial_x E_y &= 0 \quad \text{in } \Omega \times I, \\ \epsilon \partial_t E_x - \partial_y H_z &= 0 \quad \text{in } \Omega \times I, \\ \epsilon \partial_t E_y + \partial_x H_z &= 0 \quad \text{in } \Omega \times I, \\ \partial_x E_x + \partial_y E_y &= 0 \quad \text{in } \Omega \times I \end{aligned} \tag{21}$$

with the associated boundary, initial conditions and

$$\hat{n}_x E_y^+ - \hat{n}_y E_x^+ = 0 \quad \text{on } \Gamma \times I \tag{22}$$

as the embedded boundary condition for Ω^+ . From a CFM point of view, TE_z problem (21) is more challenging than TM_z problem (17) because there is no condition on the embedded boundary for the magnetic field component H_z . We therefore must heavily rely on fictitious interfaces to estimate the correction function of H_z and choose c_f large enough. On the other hand, as discussed in Sect. 3.1 and shown in Sect. 6.2.1, c_f must be chosen small enough to avoid stability problems. Hence, CFM-FDTD schemes for TE_z problem (21) with embedded boundary condition (22) may exhibit stability issues, particularly for long time simulations and very refined mesh grids. Nevertheless, we provide some numerical results for a circular cavity problem and a scattering problem in the following.

For the TE_z mode and the mesh grid presented in Sect. 6.1, the z -component of the magnetic field is approximated at the center of the cell while the x -component and y -component of the electric field are approximated respectively at $(x_i, y_{j+1/2})$ and $(x_{i+1/2}, y_j)$. We consider both the CFM-Yee and CFM-4th schemes. The error of $\mathbf{U} = [E_x, E_y, H_z]^T$ at t_n is computed using approximations and analytic solutions of the magnetic field and the electric field at respectively $t_n - \frac{\Delta t}{2}$ and t_n because of the staggered grid in time.

Let us first begin with a circular cavity problem. The domain of this problem is the same as in the TM_z mode circular cavity problem. In subdomain Ω^+ , the solution in cylindrical

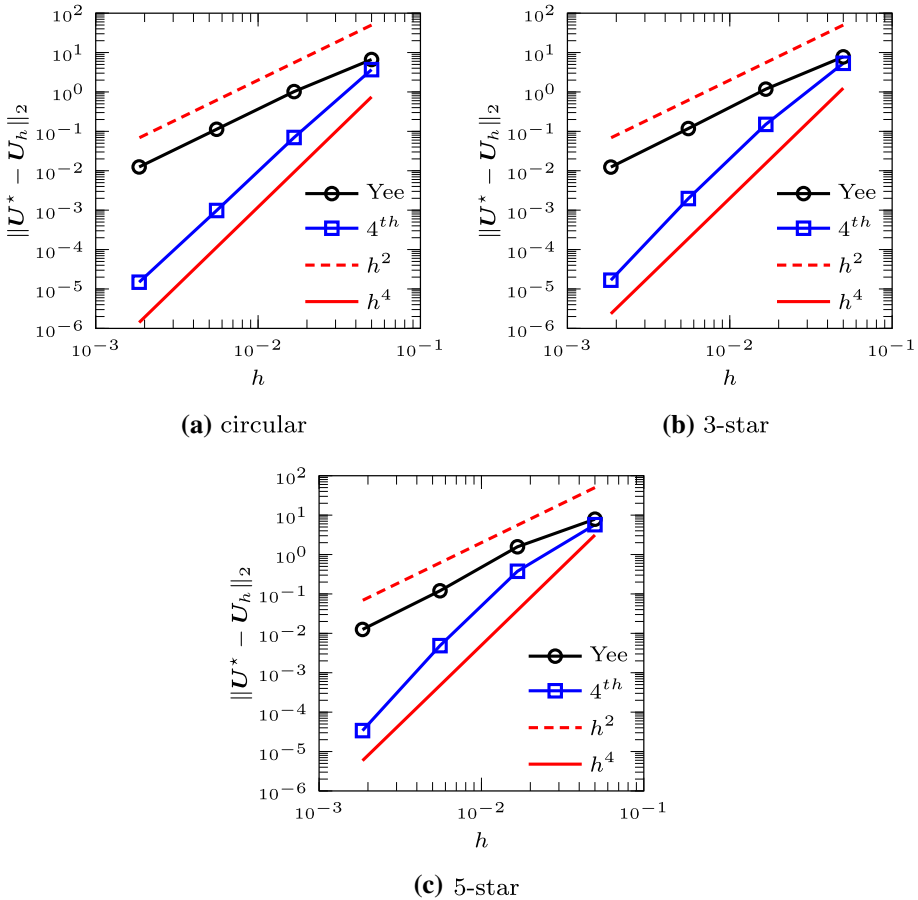


Fig. 12 Convergence plots in L^2 -norm for TM_z scattering problems using the proposed CFM-FDTD schemes and different geometries of the embedded PEC

coordinates is given by

$$E_\rho^+(\rho, \phi, t) = \frac{i}{\alpha_{i,j} \rho} J_i(\alpha_{i,j} \rho) \sin(i \phi) \sin(\alpha_{i,j} t),$$

$$E_\phi^+(\rho, \phi, t) = \frac{1}{2} (J_{i-1}(\alpha_{i,j} \rho) - J_{i+1}(\alpha_{i,j} \rho)) \cos(i \phi) \sin(\alpha_{i,j} t),$$

$$H_z^+(\rho, \phi, t) = -J_i(\alpha_{i,j} \rho) \cos(i \phi) \cos(\alpha_{i,j} t),$$

where $\alpha_{i,j}$ is the j -th positive real root of the first derivative of the i -order Bessel function of first kind $\partial_\rho J_i$. In this numerical example, we choose $i = 6$ and $j = 2$. The time interval is $I = [0, 3]$ in which five and a half periods are included. The other parameters are the same as in Sect. 6.2.1. Convergence plots, illustrated in Fig. 16a, shows a second and third order convergence for respectively the CFM-Yee scheme and the CFM-4th scheme in L^2 -norm. Let us now consider a scattering problem involving the 4-star PEC. We compute the reference solution U^* using $h = \frac{1}{540}$ and the CFM-4th scheme. The length in space of local patches is $\ell_h = 6h$. The other parameters are the same as in Sect. 6.4. The pulsed wave propagating in

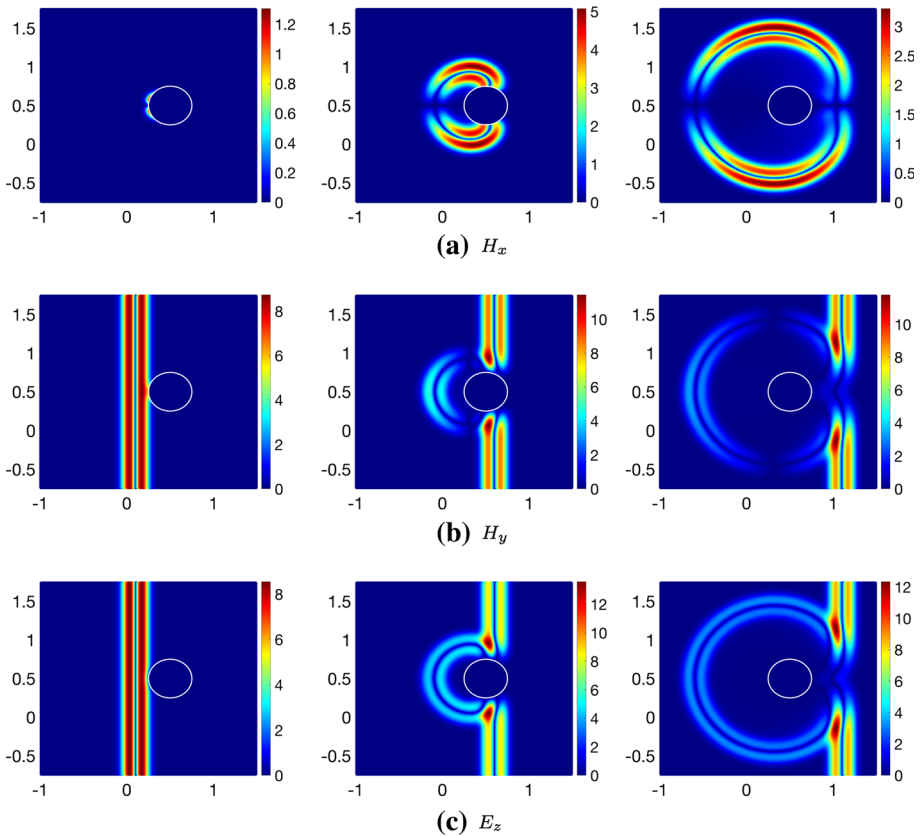


Fig. 13 The evolution of the magnitude of components H_x , H_y and E_z with $h = \frac{1}{100}$ and $\Delta t = \frac{h}{2}$ using the CFM- 4^{th} scheme and the circular embedded PEC. From left to right, we show the computed electric field and magnetic field at respectively $t \in \{0.4, 0.9, 1.4\}$ and $t - \frac{\Delta t}{2}$. The embedded boundary is represented by the white line

the positive x -direction is given by

$$\begin{aligned}
 E_{x_p}(\mathbf{x}, t) &= 0, \\
 E_{y_p}(\mathbf{x}, t) &= \frac{2}{\sigma^2} (x - \gamma - t) e^{-\left(\frac{x-\gamma-t}{\sigma}\right)^2}, \\
 H_{z_p}(\mathbf{x}, t) &= \frac{2}{\sigma^2} (x - \gamma - t) e^{-\left(\frac{x-\gamma-t}{\sigma}\right)^2},
 \end{aligned}$$

where $\sigma = 0.1$ and $\gamma = -0.3$. Figure 16b shows convergence plots for both CFM-FDTD schemes. We observe a second and third order convergence for respectively the CFM-Yee scheme and the CFM- 4^{th} scheme. Numerical results are in agreement with the theory.

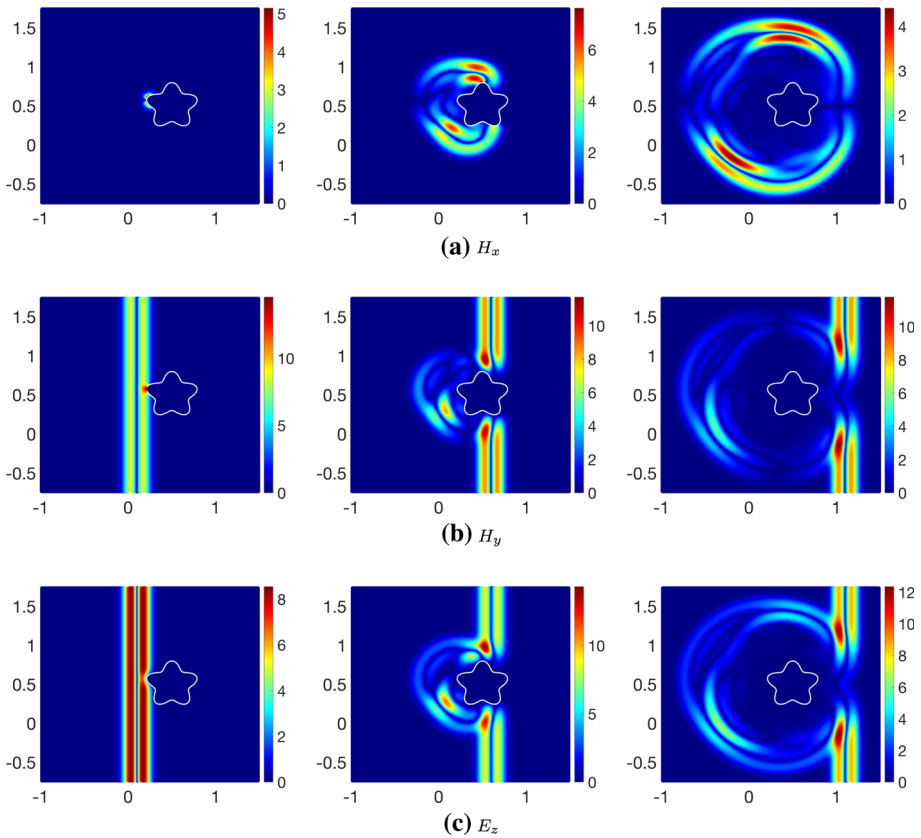


Fig. 14 The evolution of the magnitude of components H_x , H_y and E_z with $h = \frac{1}{100}$ and $\Delta t = \frac{h}{2}$ using the CFM- 4^{th} scheme and the 5-star embedded PEC. From left to right, we show the computed electric field and magnetic field at respectively $t \in \{0.4, 0.9, 1.4\}$ and $t - \frac{\Delta t}{2}$. The embedded boundary is represented by the white line

8 Conclusions

This work proposes FDTD schemes based on the Correction Function Method for Maxwell’s equations with embedded PEC boundary conditions. The associated minimization problems are well-posed for an appropriate representation of the embedded boundary within the local patch, and an appropriate choice of penalization coefficients and fictitious interfaces. However, fictitious interfaces impact the stability of a CFM-FDTD scheme, which is particularly noticeable when the TE_z mode is used. For the TM_z mode, the penalization coefficient associated with fictitious interfaces can be chosen small enough to avoid stability problems. We have applied the CFM to the well-known Yee scheme and a fourth-order staggered FDTD scheme. It is worth mentioning that the proposed numerical strategy can be implemented as a black-box to existing softwares. Based on numerical examples, it has been shown that the proposed CFM-FDTD schemes can handle embedded PEC problems with various geometries of the boundary while retaining high-order convergence and without significantly increasing the complexity of the proposed numerical approach. Future work will further investigate the stability of CFM-FDTD schemes and extend the proposed schemes in 3-D.

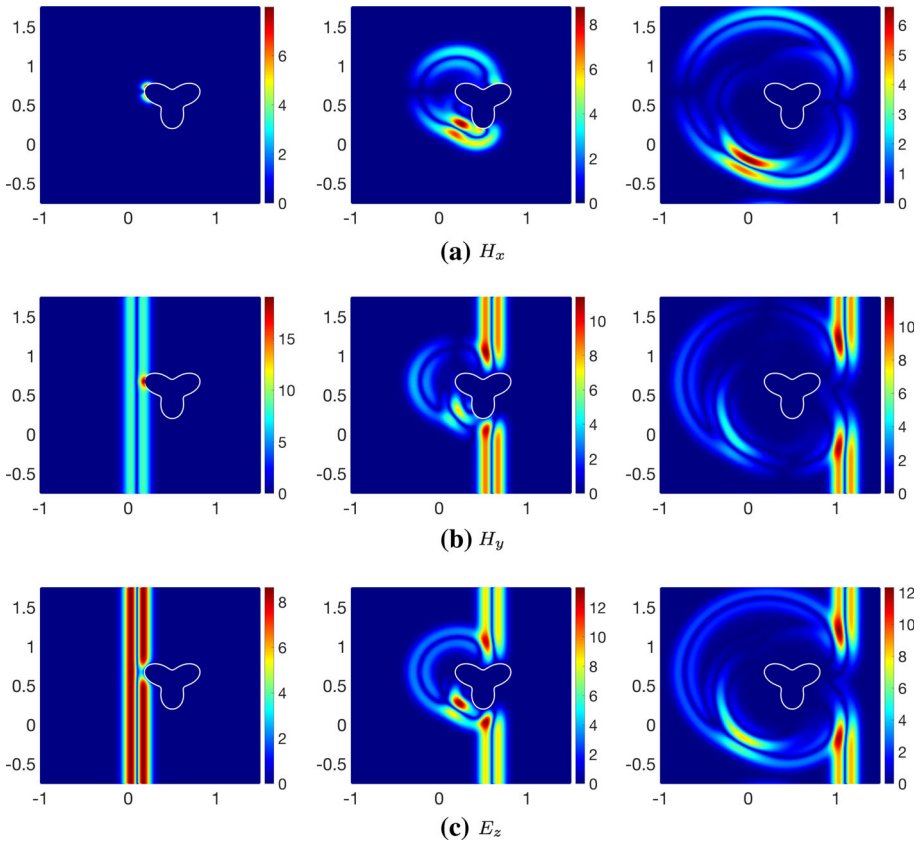


Fig. 15 The evolution of the magnitude of components H_x , H_y and E_z with $h = \frac{1}{100}$ and $\Delta t = \frac{h}{2}$ using the CFM- 4^{th} scheme and the 3-star embedded PEC. From left to right, we show the computed electric field and magnetic field at respectively $t \in \{0.4, 0.9, 1.4\}$ and $t - \frac{\Delta t}{2}$. The embedded boundary is represented by the white line

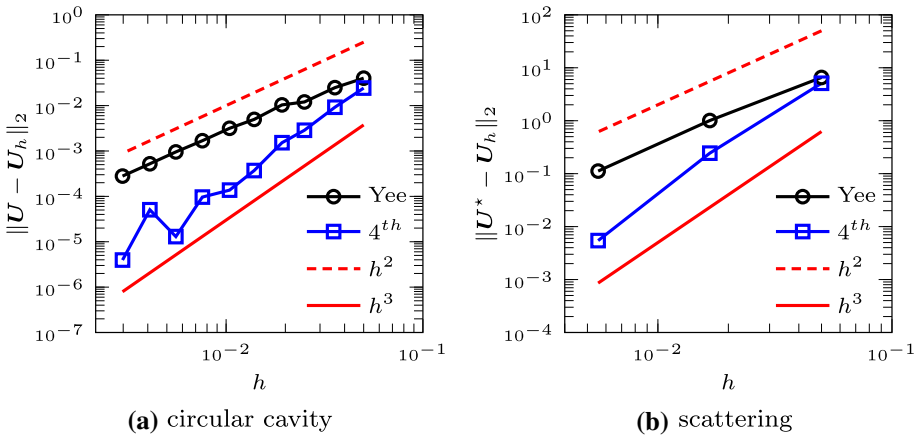


Fig. 16 Convergence plots in L^2 -norm for a circular cavity problem and the scattering of a 4-star PEC problem using the TE_z mode and the proposed CFM-FDTD schemes

Acknowledgements The authors are grateful to Dr. Marc Laforest and Dr. Serge Prudhomme of Polytechnique Montréal for their support. The authors also thank Damien Tageddine for helpful conversations.

Funding The research of JCN was partially supported by the NSERC Discovery Program.

Code availability The custom code used for this work is not yet publicly available.

Declaration

Conflict of interest The authors declare that they have no conflict of interest.

A Truncation Error Analysis

As shown in [19], the CFM can reduce the order in space of an original FD scheme for unsteady problems. Proposition 3 provides a general result on the order in space of a corrected FD scheme.

Proposition 3 *Let us consider a domain Ω , a time interval I and an interface $\Gamma \subset \Omega$ on which there are interface jump conditions. Assume that the correction function coming from the CFM is smooth enough and is such that*

$$\partial_t \hat{U} + L(\hat{U} + A \hat{D}) = F, \quad (23)$$

where \hat{U} is the vector of true solution values, A is a rectangular matrix with either 0 or ± 1 as components, \hat{D} is the vector of true correction function values, L is a spatial finite difference operator of order n that approximates q -order derivatives and F is a source term. A $(k+1)$ -order approximation of the correction function leads to a corrected FD scheme of order $\min\{n, k - q + 1\}$ in space.

Proof A $(k+1)$ -order approximation of \hat{D} leads to

$$D = \hat{D} + \mathcal{O}(\ell_h^{k+1}),$$

where $\ell_h = \beta h$ is the length of the space–time patch, β is a positive constant and h is the mesh grid size. The discrete operator L , that approximates q -order derivatives, involves components scaled by a factor $\frac{1}{h^q}$. Hence, $LA D = LA \hat{D} + \mathcal{O}(\ell_h^{k+1} h^{-q}) = LA \hat{D} + \mathcal{O}(h^{k-q+1})$. \square

For problems that do not involve transient derivatives, we have

$$\hat{U} = L^{-1} F - A \hat{D}$$

and the order of the corrected FD scheme is then $\min\{n, k + 1\}$.

References

1. Abraham, D.S., Giannacopoulos, D.D.: A parallel implementation of the correction function method for Poisson's equation with immersed surface charges. *IEEE Trans. Magn.* **53**(6), 1–4 (2017)
2. Abraham, D.S., Marques, A.N., Nave, J.C.: A correction function method for the wave equation with interface jump conditions. *J. Comput. Phys.* **353**, 281–299 (2018)
3. Assous, F., Ciarlet, P., Labrunie, S.: *Mathematical Foundations of Computational Electromagnetism*. Springer, Berlin (2018)
4. Chen, Z., Wang, L., Zheng, W.: An adaptive multilevel method for time-harmonic Maxwell equations with singularities. *SIAM J. Sci. Comput.* **29**, 118–138 (2007)

5. Chen, Z., Xiao, Y., Zhang, L.: The adaptive immersed interface finite element method for elliptic and Maxwell interface problems. *J. Comput. Phys.* **228**, 5000–5019 (2009)
6. Cockburn, B., Li, F., Shu, C.W.: Locally divergence-free discontinuous Galerkin methods for the Maxwell equations. *J. Comput. Phys.* **194**(2), 588–610 (2004)
7. Cohen, G., Ferrieres, X., Pernet, S.: A spatial high-order hexahedral discontinuous Galerkin method to solve Maxwell's equations in time domain. *J. Comput. Phys.* **217**, 340–363 (2006)
8. Ditkowski, A., Dridi, K., Hesthaven, J.S.: Convergent Cartesian grid methods for Maxwell equations in complex geometries. *J. Comput. Phys.* **170**, 39–80 (2001)
9. Fan, G.X., Liu, Q.H., Hesthaven, J.S.: Multidomain pseudospectral time-domain simulations of scattering by objects buried in lossy media. *IEEE Trans. Geosci. Remote Sens.* **40**, 1366–1373 (2002)
10. Galagusz, R., Shirokoff, D., Nave, J.C.: A Fourier penalty method for solving the time-dependent Maxwell's equations in domains with curved boundaries. *J. Comput. Phys.* **306**, 167–198 (2016)
11. Ghrist, M., Fornberg, B., Driscoll, T.A.: Staggered time integrators for wave equations. *SIAM J. Numer. Anal.* **38**, 718–741 (2000)
12. Gustafsson, B., Kreiss, H.O., Olinger, J.: *Time-Dependent Problems and Difference Methods*. Wiley, London (1995)
13. Hesthaven, J.S.: High-order accurate methods in time-domain computational electromagnetics: a review. *Adv. Imag. Electron Phys.* **127**, 59–123 (2003)
14. Hesthaven, J.S., Warburton, T.: Nodal high-order methods on unstructured grids: I. Time-domain solution of Maxwell's equations. *J. Comput. Phys.* **181**, 186–221 (2002)
15. Hesthaven, J.S., Warburton, T.: *Nodal Discontinuous Galerkin Methods?: Algorithms, Analysis, and Applications*. Springer, New York (2008)
16. Inan, U.S., Inan, A.S., Said, R.K.: *Engineering Electromagnetics and Waves*. Pearson, London (2014)
17. Jurgens, T.G., Taflove, A., Umashankar, K., Moore, T.G.: Finite-difference time-domain modeling of curved surfaces. *IEEE Trans. Antennas Propag.* **40**, 357 (1992)
18. Kallemov, B., Bhalla, A.P.S., Griffith, B.E., Donev, A.: An immersed boundary method for rigid bodies. *Commun. Appl. Math. Comput. Sci.* **11**, 79–141 (2016)
19. Law, Y.M., Marques, A.N., Nave, J.C.: Treatment of complex interfaces for Maxwell's equations with continuous coefficients using the correction function method. *J. Sci. Comput.* **82**(3), 56 (2020)
20. Marques, A.N., Nave, J.C., Rosales, R.R.: A correction function method for Poisson problems with interface jump conditions. *J. Comput. Phys.* **230**, 7567–7597 (2011)
21. Marques, A.N., Nave, J.C., Rosales, R.R.: High order solution of Poisson problems with piecewise constant coefficients and interface jumps. *J. Comput. Phys.* **335**, 497–515 (2017)
22. Marques, A.N., Nave, J.C., Rosales, R.R.: Imposing jump conditions on nonconforming interfaces for the correction function method: a least squares approach. *J. Comput. Phys.* **397**, 108869 (2019)
23. Stein, D.B., Guy, R.D., Thomases, B.: Immersed boundary smooth extension: a high-order method for solving PDE on arbitrary smooth domains using Fourier spectral methods. *J. Comput. Phys.* **304**, 252–274 (2016)
24. Wang, J., Yin, W.: Development of a novel FDTD (2,4)-compatible conformal scheme for electromagnetic computations of complex curved PEC objects. *IEEE Trans. Antennas Propag.* **61**, 299–309 (2013)
25. Wang, L., Hou, S., Shi, L., Zhang, P.: A numerical method for solving the variable coefficient wave equation with interface jump conditions. *Int. J. Numer. Anal. Model.* **16**, 1–17 (2019)
26. Yang, B., Gottlieb, D., Hesthaven, J.S.: Spectral simulations of electromagnetic wave scattering. *J. Comput. Phys.* **134**, 216–230 (1997)
27. Yee, K.S.: Numerical solution of initial boundary value problems involving Maxwell's equations in isotropic media. *IEEE Trans. Antennas Propag.* **14**(3), 302–307 (1966)
28. Yee, K.S., Chen, J.S., Chang, A.H.: Conformal finite difference time domain (FDTD) with overlapping grids. *IEEE Trans. Antennas Propag.* **40**, 1068 (1992)
29. Yu, S., Zhou, Y., Wei, G.W.: Matched interface and boundary (MIB) method for elliptic problems with sharp-edged interfaces. *J. Comput. Phys.* **224**, 729–756 (2007)
30. Zhang, Y., Nguyen, D.D., Du, K., Xu, J., Zhao, S.: Time-domain numerical solutions of Maxwell interface problems with discontinuous electromagnetic waves. *Adv. Appl. Math. Mech.* **8**, 353–385 (2016)
31. Zhao, S.: A fourth order finite difference method for waveguides with curved perfectly conducting boundaries. *Comput. Methods Appl. Mech. Eng.* **199**, 2655–2662 (2010)
32. Zhao, S., Wei, G.W.: High-order FDTD methods via derivative matching for Maxwell's equations with material interfaces. *J. Comput. Phys.* **200**, 60–103 (2004)